2014

Effects of Relaxed Assumptions on the State Switching Technique

Stephen Ilardi
University of Central Florida

EFFECTS OF RELAXED ASSUMPTIONS ON THE STATE SWITCHING TECHNIQUE

by

STEPHEN J. ILARDI

A thesis submitted in partial fulfillment of the requirements
for the Honors in the Major in Mechanical Engineering
in the College of Engineering and Computer Science
and in the Burnett Honors College
at the University of Central Florida
Orlando, FL

Summer Term 2014

Thesis Chair: Dr. Jeffrey L. Kauffman

ABSTRACT

This thesis explores the effects of two assumptions commonly used in mathematical models related to a piezoelectric damping method known as State Switching. The technique relies on changing the stiffness state of a piezoelectric patch through control of the electrical boundary conditions. The transition between stiffness states is assumed to occur instantaneously and in concurrence with the switch event. In actuality, the transition will occur over a finite time and will trail behind the switch event by a finite time. For these assumptions to be valid, the effects of switch duration and delay on the performance of the State Switching method must be examined. The vibration reduction for various switch duration/delay values was calculated using a numerical solver; the results of the simulations were used to provide a range in which the two aforementioned assumptions produce negligible error, defined here as a 10% decrease in method performance. Switch durations of more than 3% of the forcing period lead to significant performance decrease, for most values of damping and coupling coefficient. Results of the switch delay simulations were counter-intuitive and require further examination and validation.

ACKNOWLEDGEMENTS

I would like to recognize the staff of the MMAE department for the role they have played in my academic career. Special thanks to Dr. Ali Gordon who first approached me regarding Undergraduate research and led me to my Thesis Chair. I would also like to thank the Burnett Honors College and staff, through whom the HIM Thesis program is made possible.

Thank you to my Thesis Committee members, Dr. Tuhin Das and Dr. Raj Vaidyanathan for challenging my knowledge of the material with thought-provoking questions and for their part in making the thesis defense process enjoyable.

Thank you to my Thesis Chair, Dr. Jeffrey L. Kauffman, for sacrificing time and energy required to be a committee chair. The knowledge and experience provided by Dr. Kauffman was invaluable and his attitude and work ethic inspiring.

Thank you to God for providing the grace and strength to push forward, especially when I felt entirely insufficient for the task at hand.

Finally a thank you to my church family and friends for their support through this process. And to my Dad, Mom, and Sister, for the strength and encouragement they provided.

TABLE OF CONTENTS

LIST OF FIGURES

LIST OF TABLES

CHAPTER 1: INTRODUCTION

As the focus of industrial research moves towards increased efficiency and cost-effectiveness, machinery components are becoming thinner, more lightweight, and thus more fragile than those in past decades. Examples of this trend of interest here lie in the turbomachinery-based power generation and aviation industries: thinner blades reduce drag, increase aerodynamic efficiency, and decrease weight but increase blade susceptibility to fatigue. Several methods for vibration reduction of turbomachinery blades exist; the goal of this thesis is to discuss the effects of modeling assumptions on a handful of these techniques, particularly those involving the use of piezoelectric-based state switching techniques.

1.1 INTRODUCTION TO VIBRATION

Vibration can be defined as "a periodic motion of the particles of an elastic body or medium in alternately opposite directions from the position of equilibrium when that equilibrium has been disturbed" [1]. In short, vibration is any oscillatory motion. Systems experiencing vibratory motion are often described in terms of spring-mass-damper models for simplicity; the simplest, one degree of freedom, spring-mass-damper system is shown in Figure 1 below.

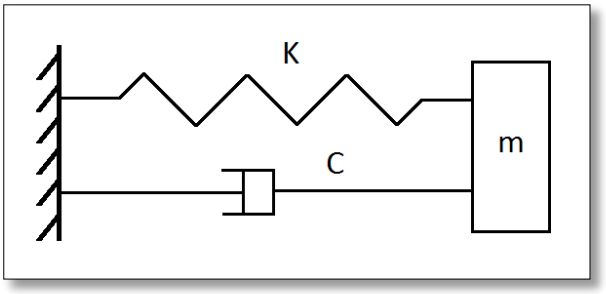

Figure 1: Single DOF Spring-Mass-Damper System

The analysis conducted in this thesis will be constrained to one mechanical degree of freedom, with an additional electrical degree of freedom. Vibration is a pervasive topic in machine dynamics, mechanics of materials, machine design, and many others. Vibration is often an unintended consequence of intended motion: for instance, the rotation of an unbalanced cam produces vibratory motion in the cam shaft which may result in the follower losing contact with the cam. In addition to hampering kinematic performance, vibration can accelerate the damage accumulation of a component. The cycle begins with the formation of microscopic cracks; the cracks act as stress amplifiers for the remaining material which leads to crack propagation [2]. Once the stress amplification due to the presence of the crack becomes too great, fracture occurs. The effects of cyclic loading on component life are often tracked using a cycles to failure diagram, or S-N plot, shown in Figure 2. These plots show the expected life of the component versus the stress amplitude.

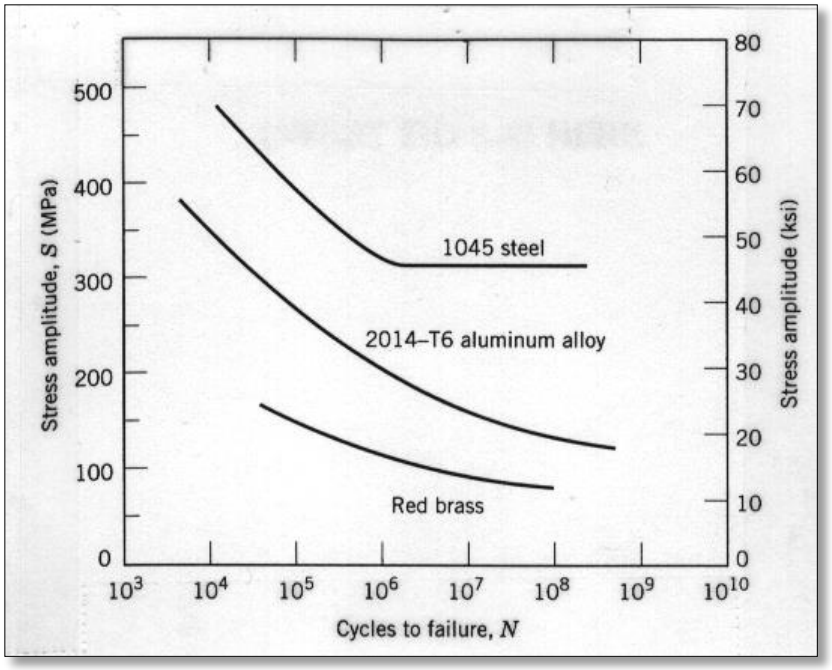

Figure 2: Typical S-N Curve for Three Materials

Reproduced without permission from [3]

1.1.1 DAMPERS

Dampers aid in limiting vibration amplitude by removing kinetic or potential energy from the system of interest. Commons methods of vibration damping include the use of lubricated or dry friction as well as tuned mass dampers and impact dampers [4]. Friction dampers convert mechanical energy to thermal energy to be dissipated into the environment; another approach is constrained layer damping. Foil tapes are commonly used in aerospace applications to deaden vibrational noise. The viscoelastic backing of the tape experiences shear stress and the 'internal friction' damps the system. Friction damping is the simplest damping method as it only requires two surfaces be in contact; frictional damping is present even when damping is not required or even desired. Tuned mass dampers reduce vibration amplitudes of one system by increasing the vibration experienced by another. These dampers can range from the seven-hundred and thirty ton

ball atop the Taipei 101 skyscraper to the four pound TMD's developed by Raytheon for use in optical assemblies to sub-gram MEMS applications [5]. Impact dampers dissipate energy through impact, as the name implies, returning only a portion of the initial kinetic energy. Current studies examine the possibility of actively controlling the impact in order to tune the damping provided by the impact damper; Afsharfard and Farshidianfar have proposed using magnetorheological fluids to tune an impact damper [6].

1.2 APPLICATIONS OF VIBRATION CONTROL

Nearly all industries require a high degree of vibration control; some that exhibit an extremely high sensitivity to unwanted vibrations are the fields of optics, electronics, and turbomachinery. Modern optics systems are capable of capturing high resolution images from several miles away or, in the case of large telescopes, from other galaxies. Small angular displacements of the camera can result in large displacements of the projected image. Electronics continue to increase in power while decreasing in size, at the same time they are becoming more fragile. Turbine blades face harsh conditions during typical operations such as high temperatures, a caustic environment, and high frequency vibrations.

1.3 TURBOMACHINERY

The damping techniques discussed in this research have been considered for application to turbomachinery due to their potential in an environment that severely restricts conventional

damping techniques. As such, vibration reduction of turbine blades will serve as an example throughout this thesis.

Bladed disks can be composed of several pieces or a single piece, known as monolithic construction. Underplatform dampers, which are discussed further in 1.3.1, or blade shrouds are often used to provide frictional damping in conventional bladed disks; frictional damping is also present at the blade root where it is attached to the central hub. On examining the bladed disk assembly, one can see that the blades constitute the weak point of the assembly. Unfortunately, monolithic disks do not admit these frictional damping approaches.

Turbine blades experience high frequency excitation during normal operation due to the non-uniform flow through the turbine. Pressure gradients in the flow can be attributed to the stator vanes, a series of static fins that keeps circumferential flow from developing as fluid passes through the turbine [7]. Figure 3, below, shows the non-uniformities caused by stator vanes in an axial fan; rotor blades are subjected to localized pressure gradients near stator vanes. In addition to vibration caused by non-uniform airflow, the blades are subjected to high radial loads due to centripetal acceleration. The combination results in high stress fluctuations that can quickly lead to fatigue.

Figure 3: Flow around Turbine Blades

Reproduced without permission from [8]

The historic solutions have been to incorporate thicker blades and to introduce additional contact points for increased friction-based damping; however, blade aerodynamics and turbine weight, among others, have suffered as a result. Reducing vibration amplitudes allows the use of thinner blades which decreases blade drag, turbine weight, and material costs. Two common approaches to vibration reduction of turbine blades exist: structural damping and friction damping.

1.3.1 FRICTION DAMPING

Friction damping is created by introducing surface contact through the aforementioned blade root joints, blade shrouds, and underplatform dampers; examples of blade root joints, shrouds, and underplatform dampers are shown in Figure 4 [9]. Design of these mechanisms requires extensive knowledge of blade dynamics to calculate energy lost to friction effects accurately. Current friction models are limited in their ability to predict energy losses due to abnormal contact conditions. These dampers experience 'stiction' in which the contacting surfaces may or may not experience relative motion depending on the normal force. The normal force

consists of static and dynamic components: the centripetal acceleration caused by the rotation of the bladed disk produces a quasi-static normal force while blade dynamics introduce dynamic forces. In some cases, the dynamic forces can even overcome the quasi-static centripetal force and the damping surfaces break contact with one another. Available models predict stick/slip and contact/no contact conditions; however, actual conditions may present all three conditions (stick/slip/no contact) at different points on adjoining surfaces. Mathematical model deficiencies often lead designers to search for additional methods of testing frictional damping systems. When designing underplatform dampers, 'rainbow tests' are often conducted to determine optimum design parameters experimentally. Underplatform dampers of varying masses are installed in a turbine whose blade dynamics are monitored during operation. From blade response designers hope to extrapolate optimum damper mass, but researchers in the field have voiced doubt in regards to the validity of 'rainbow tests', as in [10]. Sanliturk et al. indicate that data must be collected for modes that experience weak blade-to-blade damping; if this criteria is not met, experiments indicate that test data may be inconclusive.

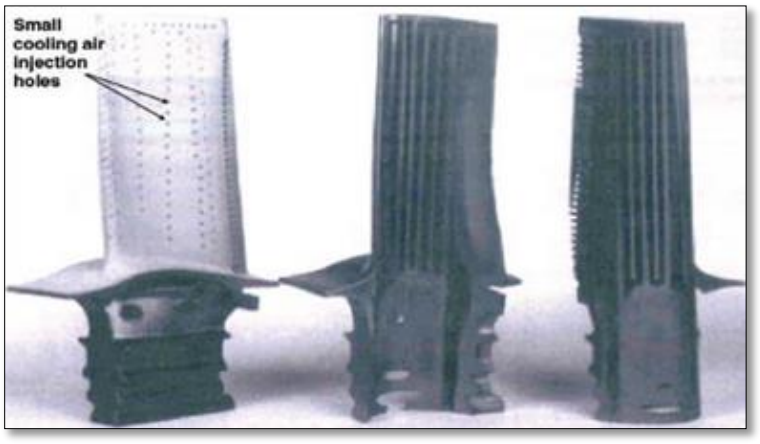

(a)

Reproduced without permission from [11]

(b)

Reproduced without permission from [12]

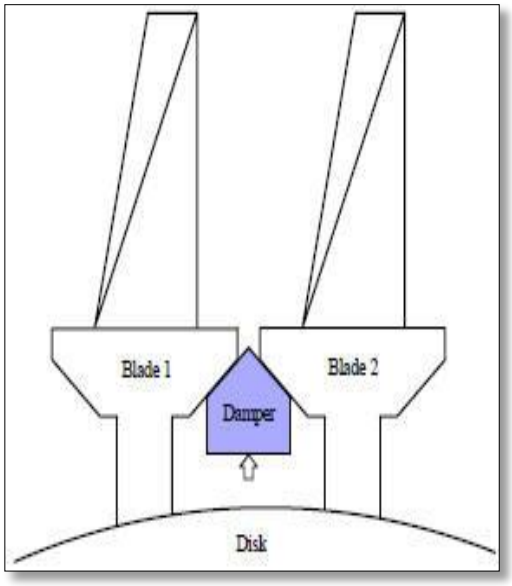

(c)

Reproduced without permission from [13]

Figure 4: Turbine Blade Friction Damping Devices

While useful, the friction damping techniques are not sufficient. Blade root/underplatform/shroud damping are only efficient for a narrow frequency band; as a result, it is necessary to augment the traditional friction damping with other damping methods [14].

1.3.2 STATE SWITCHING

The difficulties of modeling and designing friction dampers, along with the increased usage of the monolithic disk have led researchers to consider piezoelectric based techniques to supplement or replace friction damping. Damping can be achieved by varying system parameters in such a way that energy is dissipated, the most commonly varied system parameter is stiffness. Alternate stiffness states are achieved through the placement of a piezoelectric patch near a point of large deflection; piezoelectric materials are capable of an infinite number of stiffness states between the two extreme stiffness values, discussed later. The stiffness of the structure may only change by a few percent, but, when used correctly, piezoelectric patches can have a significant effect on the blade displacement amplitude. The research presented here applies to structural damping and the methods controlling the stiffness of the piezoelectric patch; these methods will be presented in detail in the State of the Art Review.

1.4 PIEZOELECTRIC MATERIALS

Piezoelectric materials are a family of crystalline solids whose mechanical and electrical properties are coupled [15]. A stress induced in the crystal causes the charged crystal structure to become unbalanced, resulting in a potential difference between two points on the crystal. The inverse is also true: an applied voltage potential induces stress in the crystal. By altering the electrical boundary conditions, the mechanical stiffness of a piezoelectric patch can be altered; with passive shunting the limiting values of non-dimensional stiffness are 1(open-circuit) and 1-k^2(short-circuit), where k^2 is the electromechanical coupling coefficient. Typical values of k^2 for piezoelectric materials can exceed 50% though for a built structure k^2 of 1-20% is more realistic.

If an electrical potential is allowed to build up in the piezoelectric material as a result of an applied stress, the material will produce an internal force that resists the applied force. Should the potential be allowed to dissipate by shorting the piezoelectric, the electromechanical properties of the piezoelectric will not factor into the patch stiffness. The piezoelectric effect and its inverse can be exploited for use in a variety of designs.

1.4.1 PIEZOELECTRIC SENSORS

The properties of piezoelectric materials allow piezoelectric sensors to be used in a wide variety of applications for which other sensors are not practical. Piezoelectric sensors are uniquely suited for use in harsh environments due to the robustness of piezoelectric materials: the combustion process in a modern automobile is monitored by a computer receiving cylinder pressure readings from a piezoelectric sensor. The size and simplicity of piezoelectric sensors has led to their use in musical instruments; sound relay boards often use piezoelectrics to convert sound waves to electrical signals. Piezoelectric materials are even present in the body: collagen is a piezoelectric material and is believed by many physicians to be a biological pressure sensor.

1.4.2 PIEZOELECTRIC ACTUATORS

Piezoelectric actuators are capable of precise motion, as a result, piezoelectrics actuators have achieved high market penetration in precision industries. Computer aided machining and additive manufacturing devices often use piezoelectric actuators to position the tooling or dispensing nozzle. Piezoelectrics have also been used in high precision suspension systems, such as those used to stabilize high magnification microscopes.

Piezoelectrics are also quite scalable, meaning that device efficiency does not decrease drastically as the device is scaled down. Several researchers have exploited the scalability of piezoelectric actuators to create medical devices previously unachievable due to geometric constraints. Valdovinos et al. produced a piezohydraulic pump for use in pediatric ventricular assist devices; such devices had previously been available to only adults and teens due to the size of the device [16].

In addition to precision motion and scalability, piezoelectric actuators are capable of operating at several thousand Hertz, this ability has been exploited to create piezoelectric stepper motors, both linear and axial. Linear piezoelectric motors are created by applying a 'step' principle to linear piezoelectric actuators. One end of an actuator is fixed and the actuator is fired, a relative displacement between the two ends of the actuator results. The free end is then fixed, the fixed end freed, and the actuator allowed to return to its normal length; this results in a net displacement of the actuator. Most office printers use linear piezoelectric motors to position inkjets. Axial piezoelectric motors use a thin piezoelectric disk, excited by a sine wave, to turn the rotor. Figure 5, below, illustrates the motion of an axial piezoelectric motor. Motor dynamics can be manipulated based on the placement of the electrodes on the piezoelectric disk; optimum electrode placement is a current area of research.

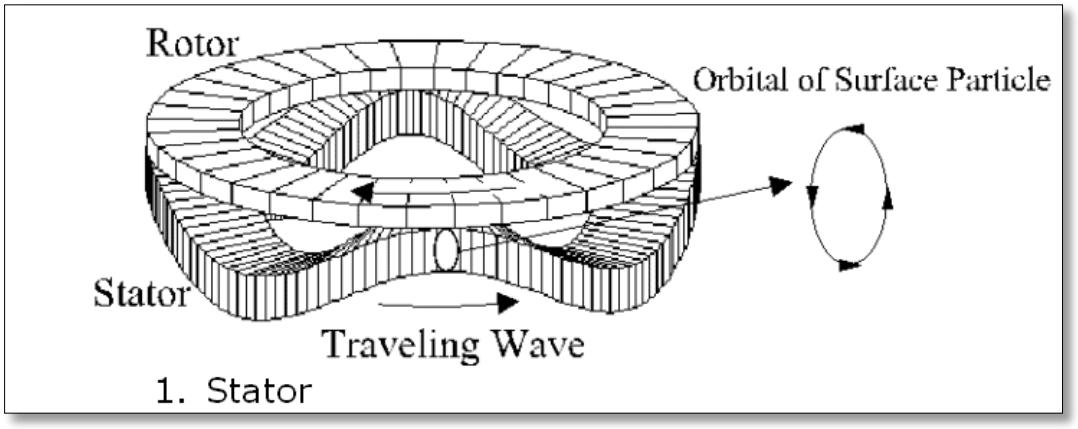

Figure 5: Piezoelectric Stator and Rotor Setup

Reproduced without permission from [17]

1.5 PROBLEM FORMULATION

Analysis of piezoelectric vibration reduction techniques often make assumptions that do not represent the physical process; the error due to these assumptions is commonly neglected in the literature. However, the true effect of these assumptions has not been explored in-depth. It is the aim of this thesis to capture the effects of common assumptions on piezoelectric damping methods.

1.5.1 INTRODUCTION TO STATE SWITCHING

State switching, as described above, pertains to the alteration of system parameters with the goal of reducing vibration; State Switching also refers to a piezoelectric based vibration reduction technique wherein the system stiffness parameter is altered. The variation in the stiffness parameter is achieved by altering the electrical boundary conditions, which in turn alters the stiffness state of the piezoelectric material. Energy is stored while the patch is in the high stiffness state and dissipated by the switch to the lower stiffness state; the switch occurs when particular events are detected in the displacement of the piezoelectric patch, specifically extrema and zeroes.

Should an event be missed or the domain transition take too long, the effectiveness of the technique may be severely hampered. For ease of analysis, the transition is typically assumed to occur instantaneously at the exact time of an event, though this is not the case.

1.5.2 PHYSICAL CONDITIONS THAT MAY CAUSE ASSUMPTION TO BE VIOLATED

There are three main factors that influence the ability of the physical system to track the ideal reference: the material, switch triggering, and switch execution. As mentioned above, no physical process occurs instantaneously; the transition from one domain to the next will require a finite amount of time. As this finite switch time consumes a greater proportion of the vibration cycle, it will reduce the effectiveness of the technique. The switch between domains is determined by a trigger that activates upon detecting an event; the trigger may introduce a delay in the domain switch. All piezoelectric based techniques require supporting circuitry; active and semi-active techniques in particular require intricate support structures. The shorting/opening of the circuit will not occur instantaneously and will act as another source of lag/switch duration.

1.5.2 PROBLEM STATEMENT

Mathematical models of piezoelectric damping techniques often assume that the stiffness state switches between two desired states instantaneously; however, no physical system is capable of instantaneous change. Under ideal conditions the patch will experience the state switch within a period of time that can be deemed negligible, but the limits of 'negligible' are not known. Non-ideal conditions may exacerbate issues caused by the instantaneous switching assumption. In order

for the instantaneous assumptions to continue in use, the results of the assumption being incorrect must be understood.

As an example, assume a given device is capable of detecting a switching second within 1 μs, and capable of carrying out the switch in an equal amount of time. The vibration period must be approximately 1.5 orders of magnitude greater than the time from switch event to switch completion. Using these parameters, the device is limited to vibrations below ~50kHz, which is quite low compared to frequencies seen in turbomachinery.

1.6 THESIS OUTLINE

The goal of this introduction is to orient the reader and to lay the ground work for in-depth discussion of piezoelectric based damping techniques. The following chapter presents and discusses previous work related to the topic, specifically piezoelectric-based vibration reduction techniques and the effects of relaxed assumptions. The third and fourth chapters present the development of the model and the procedures used during simulation. The thesis concludes with a discussion of the simulation results and summary, as well as suggestions regarding future work.

CHAPTER 2: STATE OF THE ART REVIEW

A discussion of the common piezoelectric damping techniques will best frame the research presented in this thesis. Piezoelectric-based vibration reduction techniques can be split into three categories: passive, semi-active, and active. Each method presents benefits over the others, and each method presents unique obstacles. Active techniques require the use of a power source, making these techniques unfeasible for use in small, isolated, or otherwise geometrically constrained devices, such as those used to damp turbine blades. As such active techniques will not be considered here. Passive techniques provide simplicity at the cost of a limited efficiency range, and semi-active techniques sacrifice a degree of simplicity for a wider operating range.

2.1 PASSIVE TECHNIQUES

Passive piezoelectric-based damping techniques do not require any power input to operate, thus making them good candidates for use in applications where the piezoelectric patch will be isolated. Passive circuits must be tuned to a particular frequency for maximum damping which presents a problem in systems where the excitation frequency is not constant or where multiple frequencies are of interest [18]. Outside of the narrow band, the performance of passive techniques suffers. In [19], Moheimani introduces the idea of several tuned circuits connected to a single patch; each circuit is regulated by a band-pass filter that prevents the circuit from hampering performance for non-optimal frequency ranges. As shunts are added, size, weight, and complexity become a concern. Many applications cannot accommodate the circuitry required to damp several modes passively.

2.2 SEMI-ACTIVE TECHNIQUES

Unlike passive methods, semi-active techniques require that small amounts of power be supplied to the controlling circuitry, for example to control the electrical boundary conditions of the piezoelectric patch. By controlling these boundary conditions, the patch stiffness can be altered. These techniques are more practical than passive methods for low frequencies, relative to system natural frequency, where system response is dominated by stiffness [20]. Semi-active techniques have become more popular in recent years due to their robustness: semi-active methods are significantly less dependent on excitation frequency than are the passive methods. Semi-active methods also provide the opportunity to alter the response of the piezoelectric patch as the excitation frequency changes. The semi-active family of techniques has several drawbacks, mainly the need for an external power source and a sensor to detect the triggering events that govern the switching of the electrical boundary conditions. The piezoelectric patch itself may be used to meet these needs by means of energy harvesting and monitoring displacement of the patch to trigger events. There are a plethora of semi-active techniques; four of the more prevalent are discussed below.

2.2.1 STATE SWITCHING

Clark first proposed the State Switching method as a means to combine the simplicity of passive circuits with the performance of the active techniques [20]. The stiffness state of the patch follows the heuristic control law defined by Equation (1).

$$S = \begin{cases} 1 & if\ y\dot{y} \geq 0 \\ 1 - k^2 & if\ y\dot{y} < 0 \end{cases} \quad (1)$$

Figure 6 presents a graphical illustration of State Switching. The stiffness state of the patch is determined by the location of displacement maximums, minimums, and zeroes. The patch begins in the low stiffness state and switches to the high state when the displacement equals zero; the patch returns to the low stiffness state when the displacement amplitude reaches a maximum.

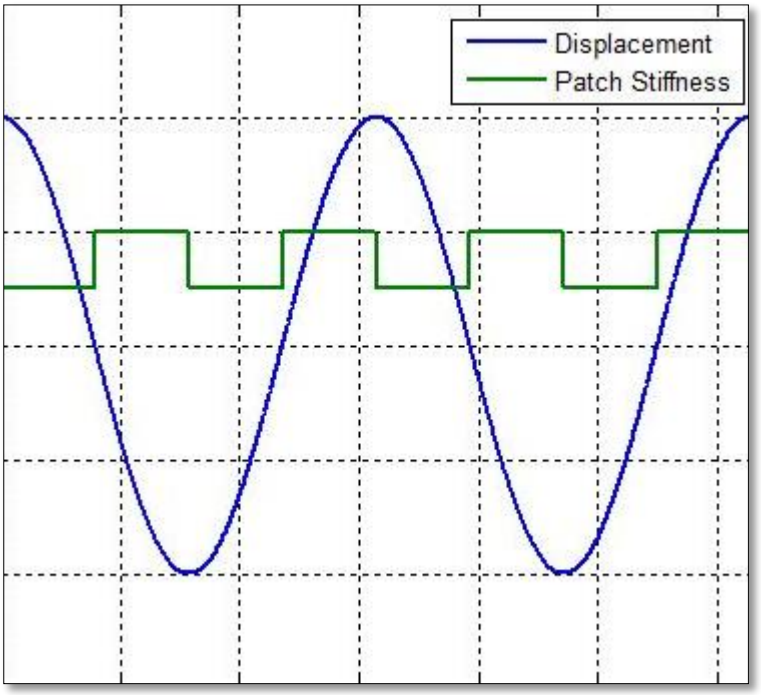

Figure 6: Patch Stiffness and Displacement versus Time

In Equation (1), S represents a normalized stiffness, y is the patch displacement, and the constant k represents the electromechanical coupling coefficient: the development of these terms will be discussed later in Model Development. The piezoelectric patch is in the open-circuit configuration when the patch is receiving energy from the system and shorted when the patch starts to give energy back to the system; the energy stored in the patch is dissipated by shorting the circuit in a manner analogous to shorting a capacitor. The two cases, receiving and returning energy, correspond to motion away from and towards equilibrium, respectively; i.e., the material is stiffer when moving away from equilibrium and softer on the return. Clark determined that this method

performed best when switching between open-circuit and a resistive shunt rather than a full short; replacing the full short with a resistive shunt produced an increase in the effective damping ratio of nearly 60%. Analytical and experimental testing have shown that the State Switching technique outperforms the passive resistive shunt in the low frequency domain where response is dominated by stiffness. The State Switching technique, however, is outperformed by the passive resistive shunt in handling transient vibrations.

2.2.2 SYNCHRONIZED SWITCHED DAMPING

The term Synchronized Switched Damping (SSD) describes a control method developed by Richard et al. in 1999 [21]. The SSD technique was proposed as an alternative to passive circuits for low frequency excitations. In this technique, the maximum vibration amplitude triggers the state switching of the piezoelectric material. Upon reaching maximum amplitude, the patch is shorted and then immediately returned to the open-circuit state; maximum displacement means maximum energy storage in the patch, with the energy then dissipated by shorting the circuit. Shorting the circuit and immediately returning it to the open-circuit state produces an interesting voltage profile, shown in Figure 7 below, which shows the slow accumulation and rapid dissipation of the electric potential.

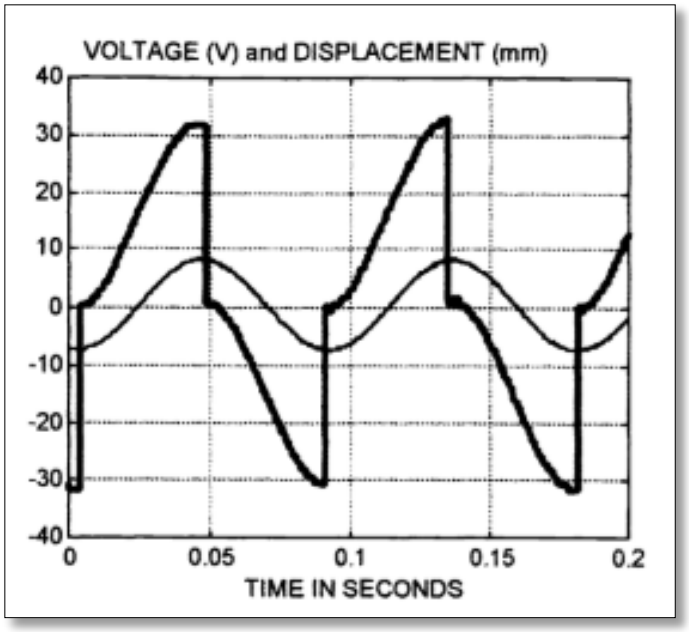

Figure 7: Synchronized Switch Damping

Reproduced without permission from [21]

While in the open-circuit state, the voltage profile follows the displacement indicating that the damping is related to the system velocity, from this Richard et al. concluded that SSD would act as a controllable viscous damper [21]. The experimental results appear similar to those achieved by a viscous damper: amplitude reduction and the introduction of a phase lag.

2.2.3 SYNCHRONIZED SWITCHED DAMPING ON AN INDUCTOR

Richard et al. improved on the Synchronized Switched Damping technique by adding an inductor to the shunt [22]. Much like the original SSD method, the Synchronized Switched Damping on an Inductor (SSDI) method waits in the open-circuit state until a pre-determined point at which the piezoelectric patch is shunted across an inductor. Instead of the potential dropping to zero, the addition of the inductor inverts the voltage, though not completely as the shunt contains a certain resistance. Inverting the voltage effectively inverts a portion of the energy stored in the

patch for the purpose of counteracting the kinetic energy of the system, as opposed to simply dissipating the energy as in the SSD method. Lefeuvre et al. proposed adding a voltage source to combat the losses due to shunt resistance; adding the power source increased damping but also transformed a semi-active method into an active method [23]. The typical voltage profile for the SSDI method is shown in Figure 8. The voltage experienced by the piezoelectric patch is much higher than the potentials seen in the original SSD approach, and as a result, the SSDI method outperforms its predecessor. In experimentation, Richard et al. achieved a 90% vibration amplitude reduction on a steel beam using the SSDI approach.

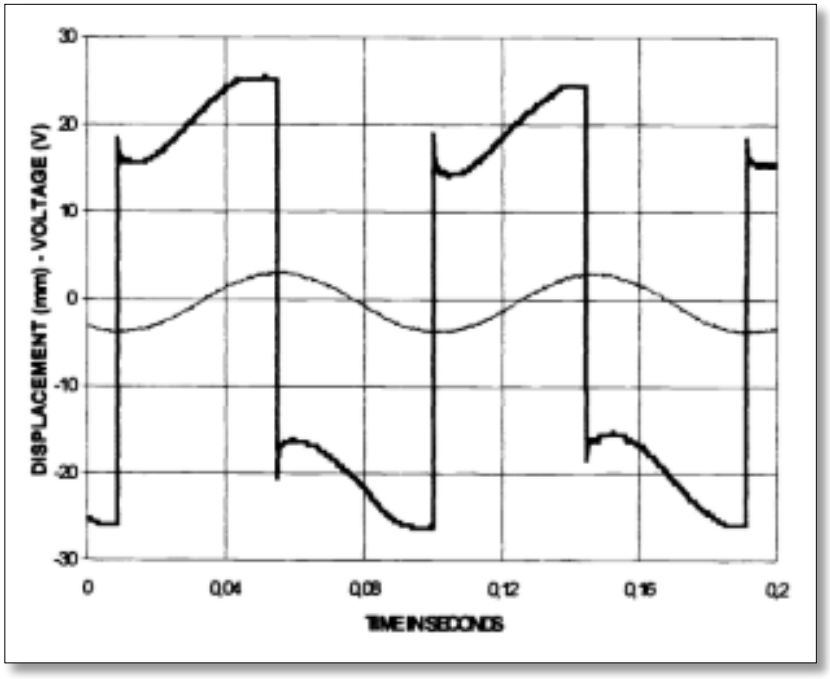

Figure 8: Synchronized Switch Damping on an Inductor

Reproduced without permission from [22]

When designing the shunt, components must be carefully selected. The voltage inversion occurs over half the period of the shunt circuit; the period of the shunt circuit must be significantly smaller than that of the system oscillations in order for the instantaneous inversion assumption to

hold. The return to open-circuit boundary conditions also occurs over half the period of the shunt circuit.

Clark et al. compared the State Switching and SSD family of techniques and determined that the SSDI method will outperform the State Switching method; however, this outcome may not be true for all circumstances; in cases where the piezoelectric patch stiffness dominates the system stiffness, the State Switching method will outperform the SSDI method [24]. Clark also noted that the SSDI method exhibits the performance of the classic resonant resistive shunt without requiring a large inductor at low frequency.

2.2.4 RESONANCE FREQUENCY DETUNING

Kauffman and Lesieutre first proposed Resonance Frequency Detuning in [25]. This method was designed to operate in the transient conditions of turbine run-up or run-down; in these operating domains the blades are subjected to a frequency sweep excitation. Blades pass through several resonance frequencies on start-up and shut-down, as well as during transient changes in operating speed, producing large vibration amplitudes which decreases blade life. A Campbell diagram is commonly used to track the resonance crossings of a turbine blade, one is presented in Figure 9. The vertical axis represents excitation frequency, the horizontal rotation speed, the grey lines various vibration modes, and the blue lines various engine orders; resonance occurs at the intersection of the blue and grey lines.

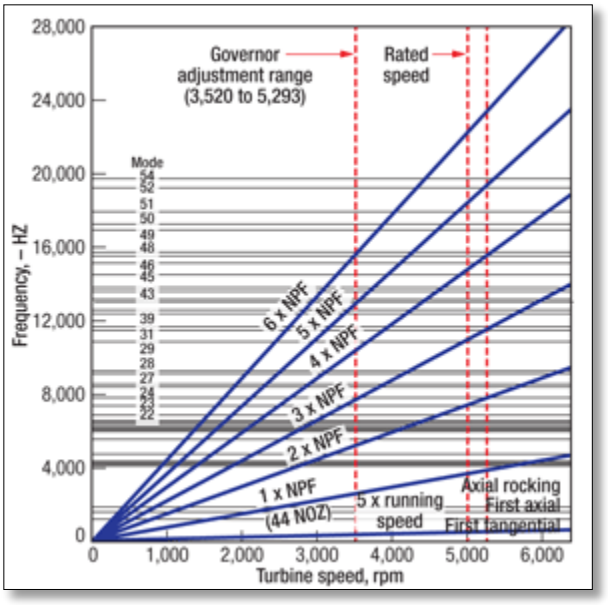

Figure 9: Typical Campbell Diagram for Blade Resonance

Reproduced without permission from [26]

Resonance frequency detuning utilizes a piezoelectric patch to create two system states, with two natural frequencies. On system start-up, the piezoelectric patch is placed in the open-circuit configuration, presenting a high stiffness value. At a pre-determined frequency associated with a resonance crossing, ω_{switch} the patch is switched to short-circuit; once resonance has passed, the patch is returned to the open-circuit state. Figure 10 presents a graphical representation of resonance frequency detuning.

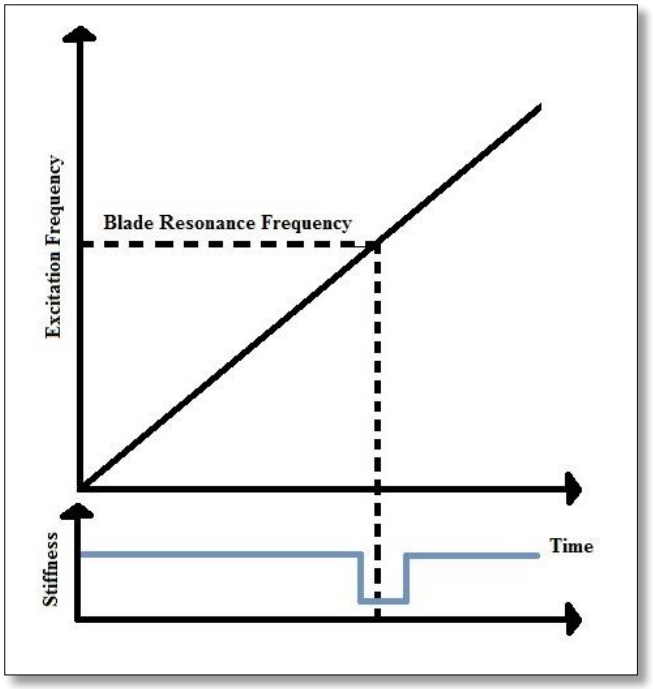

Figure 10: Resonance Frequency Detuning

The ideal switching frequency, ω_{switch}, is determined by the intersection of the frequency domain response of the open-circuit and short-circuit configurations [25]. Several factors affect the value of this optimal switching frequency. High centrifugal loads caused by high rotational speeds distort mode shapes and shift resonance frequencies. Campbell diagrams can be used to track resonance frequency versus engine speed and order (number of stator vanes). Kauffman and Lesieutre indicate that sweep rate, damping, and electromechanical coupling coefficient will also influence the optimal switching frequency; for linear sweeps, the sweep rate is defined according to:

$$f'(t) \text{ where } f(t) = (\alpha_0 + \alpha t) \qquad (2)$$

or simply the scalar α [25].

A big feature of the RFD method is its insensitivity to switch delays or durations: the RFD method switches twice per resonance crossing rather than 4 times per vibration period. The RFD

method performs well for systems with high electromechanical coupling, low damping, and low sweep rates. The sweep rate is particularly influential: harmonic motion assumptions do not hold for high sweep rates. For low sweep rates, it can be assumed that the system reaches steady-state conditions at each frequency step; however, high sweep rates violate the assumption of harmonic motion. The open-circuit and short-circuit frequency response curves are created under the assumption of harmonic motion; an exceedingly high sweep rate will introduce error in the open-circuit/short-circuit response curves which may lead to improper selection of ω_{switch}.

2.3 EFFECTS OF FINITE SWITCH DURATION AND DELAY

As discussed, each of these methods assumes that voltage changes occur instantaneously; in reality, however, the change occurs over some finite time period. Richard provides a typical time period, for a particular setup, of one millisecond for the potential in the patch to drop from its maximum to zero [21]. And in developing the SSDI method, Richard et al. discuss the time taken to invert the voltage (half the shunt period) and the importance of circuit time characteristics on device performance [22]. Kauffman and Lesieutre also mention the possibility for sensor or switch delays to seriously alter the performance of a piezoelectric device [25]. Except for these asides, existing literature provides little information on the effects of relaxed assumptions in modeling piezoelectric damping techniques.

2.4 METHOD SELECTED FOR MODELING

Constraints demand that only one of the above methods be incorporated into the model. State Switching was selected because of the frequency with which the patch boundary conditions are switched. Richard et al. discuss the need for proper component selection in the SSDI method so as to make the shunt period quite small compared to the period of oscillation [22]. The two methods that may most benefit from analysis of switch time effects are SSD and State Switching; however, since the SSD method is often replaced by its successor, SSDI, the State Switching method was selected for modeling. Also, the State Switching method is the more fundamental of the two: simulation of the State Switching method will provide insight into all methods based on the State Switching method.

CHAPTER 3: MODEL DEVELOPMENT

To simulate the response of a time delayed State Switching system, a model must be developed to relate the relevant equations spanning vibrations, turbine dynamics, and piezoelectric electromechanical coupling. The model was created in Matlab, which helped streamline the process of model creation through the use of built-in solvers. The mathematics involved are presented below along with a discussion of the model design.

3.1 VIBRATION EQUATIONS OF MOTION

The vibration of a single degree of freedom system can be described by the second order differential equation:

$$m\ddot{x} + c\dot{x} + kx = F(t) \tag{3}$$

Here $\ddot{x}$ and $\dot{x}$ represent time derivatives of the displacement *x(t)*; *m* represents the system mass, *c* the damping coefficient of the system, and *k* the system stiffness. To extend this to multiple degrees of freedom the mass, damping coefficient, and stiffness become the mass, damping, and stiffness matrices with *x(t)* becoming a vector that contains nodal displacements. When studying structural dynamics, a non-dimensionalized version of this equation is typically used. If the response (displacement/velocity/acceleration) is scaled by the mass to force magnitude ratio, $\frac{m}{f}$, then the standard equation given in (2) becomes:

$$\ddot{x} + 2\zeta\dot{x} + Sx = \cos(\omega t) \tag{4}$$

Where $\zeta = \frac{c}{m}$ and $S = \frac{k}{m}$. Harmonic forcing is assumed, as shown by the $\cos(\omega t)$ term on the right hand side of the equation. Nondimensionalizing the equation of motion allows the solution for a particular set of parameter values to apply to numerous physical systems.

The performance of the State Switching technique is often analyzed by comparing vibration amplitudes for two cases: viscous damping alone and viscous damping with State Switching. Equation (4) can be solved for steady state amplitude to provide the 'viscous only' reference point. Assume a sinusoidal response of the form:

$$x(t) = \cos(\omega t - \phi) \tag{5}$$

Equation (4) now becomes:

$$-X\omega^2 \cos(\omega t - \phi) - 2X\zeta\omega \sin(\omega t - \phi) + SX\cos(\omega t - \phi) = \sin(\omega t)$$

$$\text{OR} \tag{6}$$

$$X[(s - \omega^2)\cos(\omega t - \phi) - 2\zeta\omega \sin(\omega t - \phi)] = \cos(\omega t)$$

Using trigonometric relations this equation can be separated to give a system of two equations:

$$\begin{aligned} X[(s - \omega^2)\cos\phi + 2\zeta\omega\sin\phi] &= 1 \\ X[(s - \omega^2)\sin\phi - 2\zeta\omega\cos\phi] &= 0 \end{aligned} \tag{7}$$

Solving these equations and substituting S = 1, the high stiffness state value, gives the steady state amplitude:

$$X = \frac{1}{\sqrt{[(1 - \omega^2)^2 + 4\zeta^2\omega^2]}} \tag{8}$$

This equation can be used to provide a benchmark as it represents the steady-state response in the absence of piezoelectric damping.

3.2 RELEVANT TURBOMACHINERY DYNAMICS

The forcing frequency experienced by the turbine blades is proportional to the number of stator vanes present and can be determined using the equation:

$$f_{\text{exc}} = N \times f_{\text{rotor}} \quad (9)$$

In Equation (9), N is typically used to denote the number of stator vanes and f_{rotor} is the frequency at which the rotor is spinning [25]. The value N is typically called the engine order for its role in describing the excitation force. The analysis conducted will assume a single degree of freedom, and steady state harmonic force; transients and frequency sweeps will not be included in the model.

Other sources of damping, such as underplatform dampers, are not included in the model since the focus is on the State Switching method.

3.3 PIEZOELECTRIC MODELING

Piezoelectric materials exhibit coupled electrical and mechanical properties. As previously mentioned, strain begets an electric potential and vice versa. The coupling of these properties can be described by the coupled equations:

$$\ddot{x} + 2\zeta\dot{x} + x - Q = \cos(\omega t) \quad (10)$$

$$R\dot{Q} - k^2 x + Q = 0 \quad (11)$$

where $\zeta = \frac{c}{m}$, k^2 is the electromechanical coupling coefficient, cos(ωt) is the forcing function, R is the shunt resistance, and -$\dot{Q}$ is the current through the shunt [18]. Under open-circuit conditions

(when $V = 0$), the normalized stiffness of the piezoelectric becomes 1; for short-circuit conditions (when $I = 0$), the stiffness becomes $1 - k^2$.

The electromechanical coupling coefficient relates the amount of energy stored to the energy applied [27]:

$$k = \sqrt{\frac{\text{mechanical energy stored}}{\text{electrical energy applied}}}$$

OR (12)

$$k = \sqrt{\frac{\text{electrical energy stored}}{\text{mechanical energy applied}}}$$

Since it is a ratio, the coefficient does not carry any units; the electromechanical coupling coefficient is not only different for every piezoelectric material, but for every electrode placement and patch shape. As a result, the coupling coefficient must be determined for each unique situation. The coupling coefficient plays a significant role in the damping potential of the State Switching method: the coupling coefficient determines the amount of energy dissipation achievable.

3.4 SWITCH PROFILE GENERATION

To simulate a finite switch time, a profile was created to represent the patch stiffness during the switch. Three possible representations were selected: polynomial, sine, and hyperbolic tangent. The switch profile has to meet continuity requirements, so the hyperbolic tangent profile was not selected. Polynomial and sine functions are capable of meeting the continuity requirements; however, the polynomial profile was selected for the ease with which the function

can be manipulated. Future work may include finding an analytical solution to this problem; utilizing a polynomial makes differentiation and integration for an analytical solution much easier.

3.4.1 POLYNOMIAL PROFILE

The polynomial function was selected to start at the high stiffness state, S = 1, and transition to the lower stiffness state, S = 1-k^2, in a characteristic time value, τ. The function also maintains continuity of the first derivative at each end of the profile. The function was derived symbolically starting with a fourth order polynomial: a fourth order polynomial was selected to accommodate the boundary conditions imposed on the profile; both the stiffness profile and its derivative are continuous throughout. The skeleton equation is shown below:

$$S = At^3 + Bt^2 + Ct + D \quad (13)$$

By imposing the four necessary boundary conditions, the four equations below were generated:

$$S(0) = A(0)^3 + B(0)^2 + C(0) + D = 1 \quad (14)$$

$$S'(0) = 3A(0)^2 + 2B(0) + C = 0 \quad (15)$$

$$S(\tau) = A(\tau)^3 + B(\tau)^2 + C(\tau) + D = 1 - k^2 \quad (16)$$

$$S'(\tau) = 3A(\tau)^2 + 2B(\tau) + C = 0 \quad (17)$$

Solving the four equations simultaneously yields the following coefficient values:

$$A = \frac{2k^2}{\tau^3} ; B = -\frac{3A\tau}{2} ; C = 0 ; D = 1$$

This polynomial is inserted into Equation (4) for use in the model; the polynomial will only be used to describe the stiffness state for the duration of the characteristic switch time, τ, else the nominal high and low stiffness values will be used.

The coefficient values above will be used for the transition from high to low stiffness state, the coefficients will change for the transition from low to high stiffness state; however, the procedure for determining coefficients will remain the same.

A second polynomial was created to vary the circuit non-dimensional resistance, rather than directly varying the patch stiffness. The same procedures were followed using a value of 1000 for the high stiffness state and 0.001 for the low stiffness state. Below are the coefficient used for the polynomial transitioning from the low to high resistance states (nominally short-circuit and open-circuit, respectively).

$$A = -\frac{2(1000 - 0.001)}{\tau^3};\ B = -\frac{3}{2}A\tau;\ C = 0;\ D = 0.001$$

3.5 MODEL ASSEMBLY

The model can be broken into three main sections: the ODE45 solver, the equations of motion, and the event finder. Matlab documentation describes ODE45 as a method based on an explicit Runge-Kutta technique, the Dormand-Prince pair. ODE45 is applicable to a wide range of problems and provides a medium degree of accuracy. The equations of motion are specific to the solver. Initially a single solver was developed for both switch delay and finite switch time problems; however, it soon became apparent that the simplified solver may not accurately represent the system response. An additional solver was created to vary the stiffness indirectly by manipulating the resistance in Equations (10) and (11). Solvers will be referred to as the initial solver (stiffness directly varied) and coupled equation solver (coupled equations of motion).

The events finder is a sub-function of the ODE45 solver. Events are triggered when a set value reaches zero: in the State Switching method the pertinent events are triggered at displacement extrema and zeroes.

CHAPTER 4: SIMULATION PROCEDURE

The models developed will be used to simulate the time domain response of a vibratory system defined by a set of parameters. Based on the time domain response, the effects of a non-instantaneous switch and a delayed switch will be ascertained, simulations are computationally expensive; to limit time and resources required, a list of relevant parameters and important parameter values must be compiled. An expectation of the results is also useful as it can aid in preliminary model verification. This chapter will discuss the important parameters and discuss the methods used in determining the key parameter values used in simulation, as well as providing expectations for the simulation results and the conclusions that will be drawn from the final data.

4.1 KEY MODEL PARAMETERS

Each of the models developed involves four important parameters: switch duration, switch delay, electromechanical coupling coefficient, and damping. Throughout the thesis τ_s will be used for switch duration and τ_d will be used for switch delay. The characteristic switch delay τ_d is expressed as a fraction of the forcing function period and represents the time lag from the sensed switch trigger to the actual initiation of the switch. As such, it can apply to both the idealized instantaneous switch and a more realistic transition of the electric boundary conditions. As an example, there may be some small lag from the circuit that senses the switch condition (e.g., peak displacement in the piezoelectric-based state switching technique) to the point where it actually transmits the switch signal.

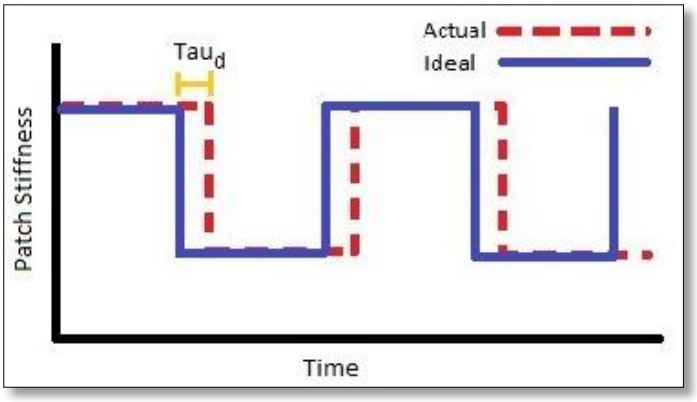

Figure 11: Characteristic Delay Time

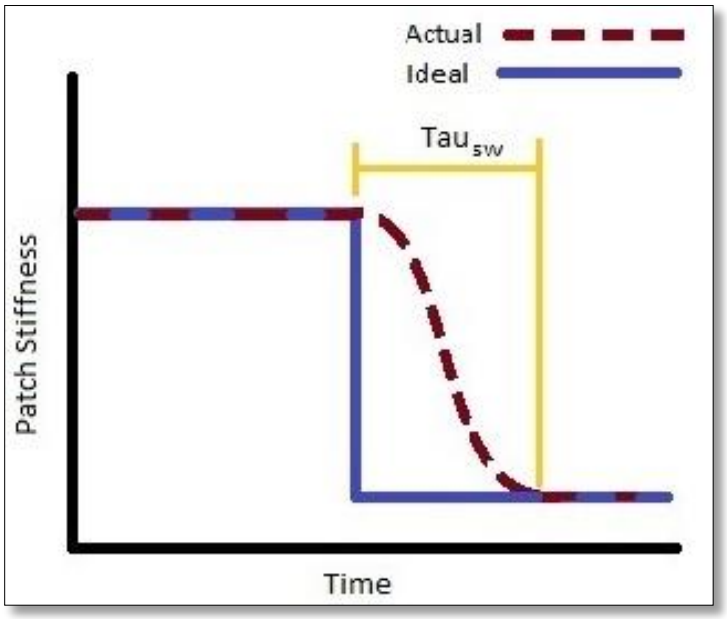

Figure 12: Characteristic Switch Time

The electromechanical coupling coefficient k^2 represents the shift between stiffness states before and after the switch. The coupling coefficient represents the overall system: the coupling coefficient of the piezoelectric patch will typically be much higher than that of the system as a whole. Both models are capable of running with several values of the coupling coefficient, even

though the coupled equation solver does not vary stiffness directly as do the other solvers; the coupled equation solver varies the circuit resistance which indirectly varies stiffness. The final parameter of interest is damping: not only will increased damping help reduce vibration amplitude, but it will likely reduce the effects of delayed switching/finite switch time, as well. The damping referred to here is the inherent damping of the system before the State Switching technique is applied.

4.2 SELECTION OF PARAMETER VALUES FOR SIMULATION

Only a finite number of parameter values can be used in simulation; values of importance were selected prior to beginning simulation. Additional values were tested upon inspection of the simulation data to fill any noticeable gaps or to further explore unexpected results. The key parameter values and the thought process behind their selection are discussed below.

4.2.1 CHARACTERISTIC TIME VALUE

The first value of the characteristic time parameter, τ_s and τ_d, is zero for all models to correspond to the idealized instantaneous assumption commonly employed and to provide a benchmark by which the following values can be evaluated. Since the stiffness state switches every quarter period, the upper limit of the characteristic time value in these simulations was twenty five percent of the forcing period. Values between zero and twenty five were spaced every 2-3% to provide a clear trend line without high computational cost. Twenty five percent was chosen as the upper limit; once the upper limit is exceeded at least one of two situations may occur, the switch

will be incomplete or the switch will occur more than 90 degrees out of phase with the triggering events.

In the case of a pure delay with instantaneous switching, once the delay is greater than twenty five percent, the stiffness state will be opposite the intended stiffness state. This results in the piezoelectric patch mechanically exciting the system rather than damping the vibration. Consider stretching a spring: first a soft spring is stretched a given distance, then a stiff spring replaces the soft spring with the same relative displacement and the stiff spring is allowed to return to its unstretched length; more energy is received from the spring than is imparted. (That is, more work is required to stretch the stiff spring than is available from returning the soft spring to its unstretched length.) In the semi-active approaches, this model result does not reflect reality as it is not possible for the patch to provide any excitation force as no power is provided directly to the patch.

In the case of a finite switch time, exceeding a twenty five percent switch time results in only partial switching. Here the patch will begin to switch stiffness states but will not complete the switch before being asked to return to the original stiffness state. In examining this problem, it is not clear how the stiffness state will vary under these conditions. It may be that the stiffness profile will be mirrored as in Figure 13 (a); upon the initial switch the stiffness state begins to decrease, and upon the secondary switch event the stiffness returns to the high state following the same line on which it descended. The stiffness profiles in Figure 13 assume the initial state is the high stiffness state; the stiffness state does not reach the low state before returning to the high state. The stiffness profile may also resemble a sinusoid that is out of phase with the switching event triggers; the sinusoidal profile is considered because it allows continuity of the derivatives. The

material properties are likely the controlling factor, as there may be domains in which the material responds differently to changes in resistance. The idea of varying response to changes in resistance lends itself better to the mirrored stiffness profile; this might be verified by modifying the coupled equations or by physical experimentation.

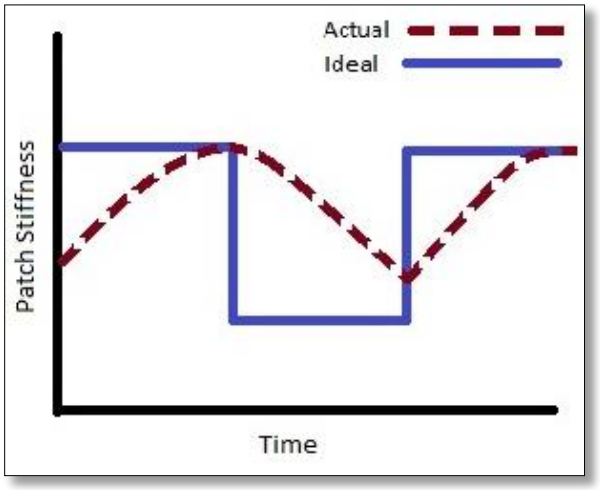

(a)

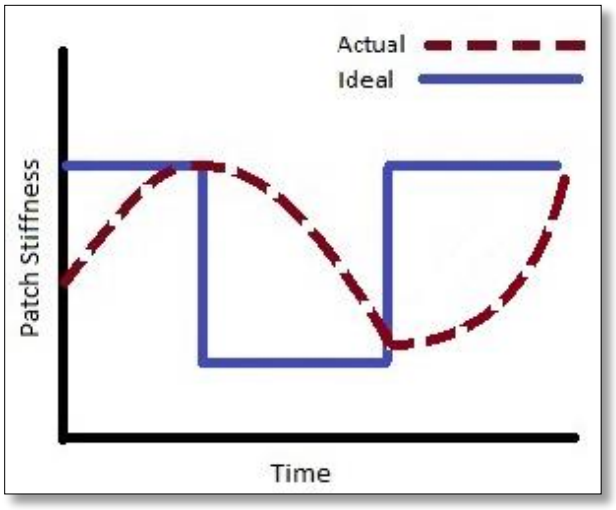

(b)

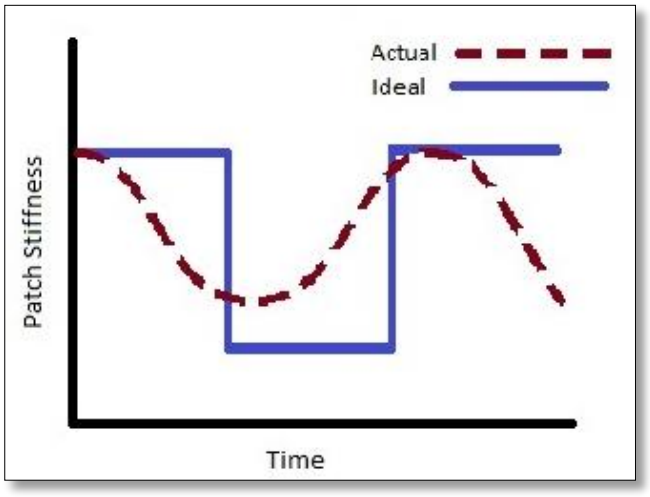

(c)

Figure 13: Possible Stiffness Profiles Beyond 25% Switch Duration

4.2.2 ELECTROMECHANICAL COUPLING COEFFICIENT

When assuming an instantaneous switch, increasing the value of the electromechanical coupling coefficient increases the damping of the technique. As switch delays and switch times are factored in, increasing the value of the coupling coefficient amplifies the effects on the system response. If adding a switch delay increases vibration amplitude, then increasing the coupling coefficient in a State Switching system where a delay is present may no longer increase damping; indeed, damping may actually be decreased. There may be an ideal coupling coefficient value for every characteristic time value that optimizes damping. The parameter values used for the electromechanical coupling coefficient were chosen to provide a wide range of values, including high and low coupling coefficients, from 1% to 50%.

4.2.3 DAMPING

Increased damping will always reduce vibration amplitude and, in the case of a non-zero characteristic time value, will aid in suppressing effects of non-ideal conditions. As such, low damping values were selected; more importantly, additional damping is not required for the high inherent damping case. Damping values range between 0.1% and 5%.

4.3 CHALLENGES ENCOUNTERED

During simulation, several problems were encountered. The simulations began with a single mathematical model; however, after examining the results it was determined that separate models must be created to handle the unique situations of a switch delay and a finite switch time. The most prevalent indicator of the model's insufficiencies was diverging results when converging results were expected. Simulations conducted with high electromechanical coupling coefficient, low damping, or high switch delay or duration often produced divergent results.

The initial model varied stiffness directly, but this approach allowed the system potential energy to increase when switching from the low to high stiffness states without the addition of energy from an external source. Adding energy to the system often produced a vibration response that increased exponentially for all time rather than a transient response followed by a final, steady-state amplitude. An example of a divergent response is shown in Figure 14: a pure switch delay of 20%, coupling coefficient of 5%, and damping of 0.1%.

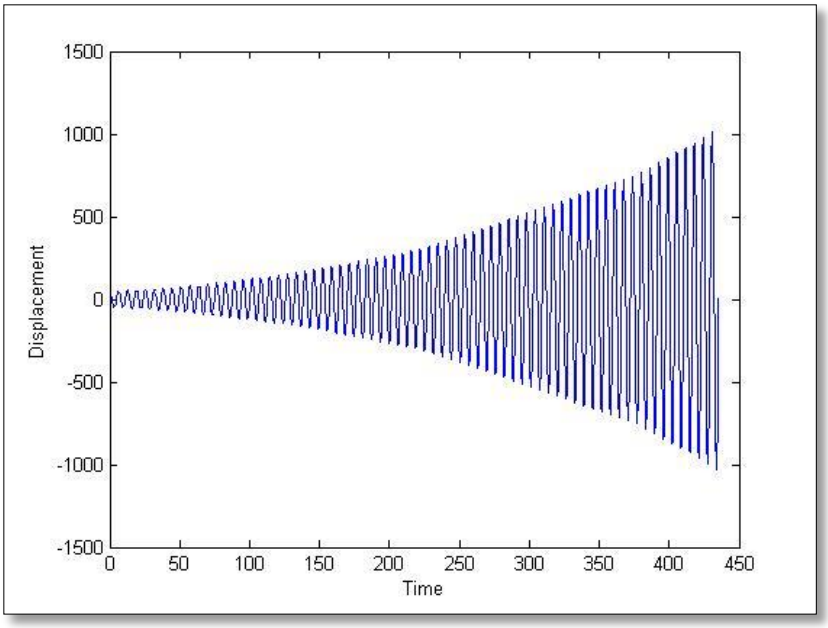

Figure 14: Divergent Response

Divergence was most prevalent in the case of pure switch delay. To combat divergence, the coupled equation solver was used to simulate pure switch delays. Although divergence was far less common in the case of a finite switch duration, the results occasionally diverged and in some cases did not resemble the expected results. As mentioned in the discussion of the characteristic time value, additional problems were encountered once the switch delay or duration exceeded 25% of the forcing function period. As the likely response of the patch to incomplete state switching is unknown, this domain was not incorporated in the simulations.

4.4 EXPECTED CONCLUSIONS FROM SIMULATION RESULTS

There are several expectations regarding conclusions to be drawn from the final results. The first is identifiable trends in steady-state vibration amplitude as the characteristic time,

electromechanical coupling coefficient, and damping are varied. From a clear trend a set of heuristics might be developed that may aid engineers in constructing semi-active damping devices. The second, and more quantifiable, conclusion to be drawn from the data is the limit at which the characteristic time value causes a significant increase in the steady-state vibration amplitude, for this study a 10% increase will be the marker of "significant" increase.

CHAPTER 5: SIMULATION RESULTS

Simulation results put quantifiable values to the ideas developed in earlier chapters. As such they are of great importance to the overall value of the research. This chapter presents a series of data representations aimed at providing a clear view of the important trends and limits of the State Switching technique as related to switch delays and finite switch time. In addition to presenting the data, some of the particularly interesting results will be examined and expounded upon; however, discussion of conclusions drawn will be saved for the next chapter.

As mentioned in Chapters 3 and 4, two models were developed for each situation: switch delay and finite switch time. For each situation, results from both models will be presented for comparison. The secondary, and more complicated, solvers can be used to evaluate the results of the simplified initial solver.

All results have been normalized by the steady-state vibration amplitude without the additional damping provided by the State Switching technique. The steady-state amplitude can be found using Equation (8) which simplifies to Equation (18) when the excitation frequency is 1 $\frac{rad}{s}$, as it is in these simulations. This value for the angular frequency was chosen because it is approximately resonance, the case in which additional damping from the State Switching method is most needed.

$$X = \frac{1}{2\zeta} \qquad (18)$$

5.1 EFFECTS OF FINITE SWITCH TIME

From the simulations run, using both the initial and the coupled equation solver, the plots below were constructed to allow the data to be easily interpreted. Separate curves represent different damping values, and each plot represents a particular value of the electromechanical coupling coefficient. Along the horizontal axis lies the characteristic time values with the vertical axis holding normalized steady state amplitudes.

As expected, the plots below indicate that the damping provided by the State Switching method decreases significantly with increasing switch duration. There are some issues with the data below that must be addressed. There are data points that appear to be outliers; however, the time domain waveforms do not indicate irregularities. An example can be seen in Figure 15; the time domain displacement response for this point is shown in Figure 16. In addition, for large values of switch duration, the decrease in performance of the State Switching method is not as great as expected.

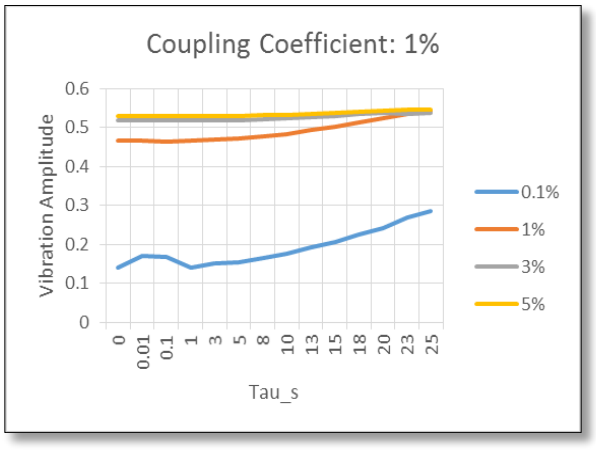

(a)

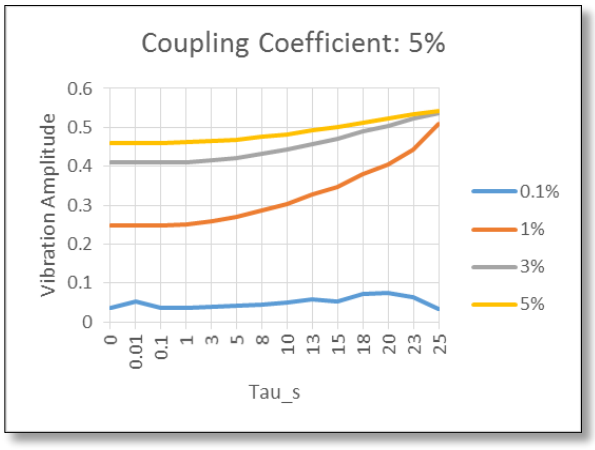

(b)

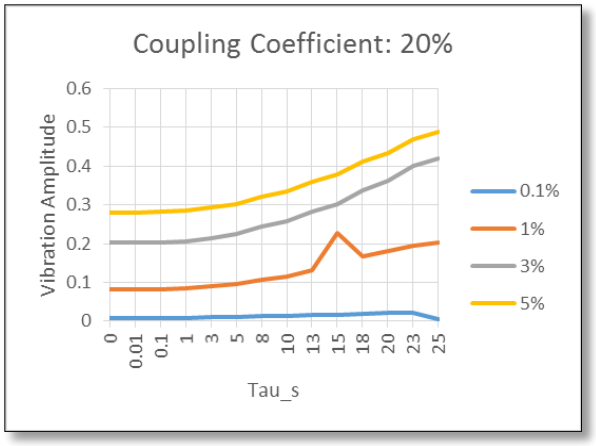

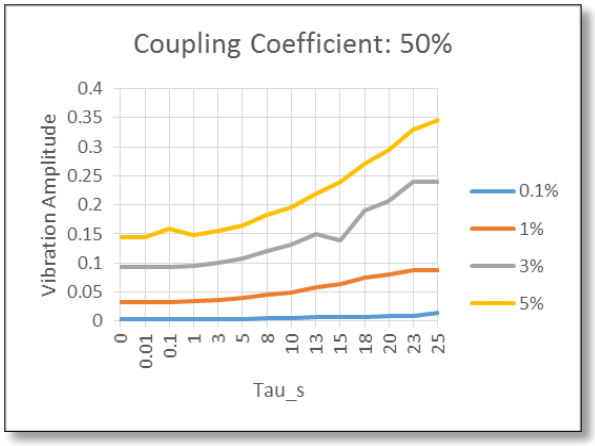

(c) (d)

Figure 15: Switch Duration Results from Initial Solver

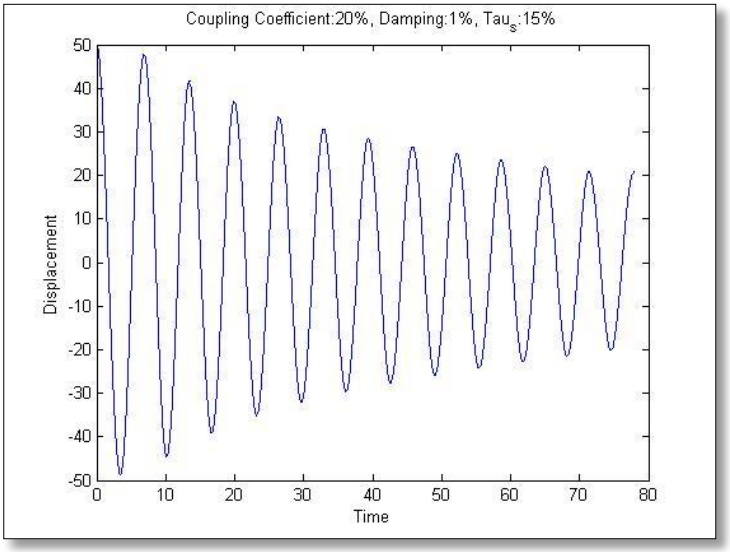

Figure 16: Time Domain Waveform for Outlier

The apparent 'outliers' and unexpected results are not, in and of themselves, reason enough to discard the data represented in the plots above; however, the disparity between the results shown above and those produced by the coupled equation solver indicates that the initial approach is

insufficient for modeling. Below are the plots presenting the results of the coupled equation results.

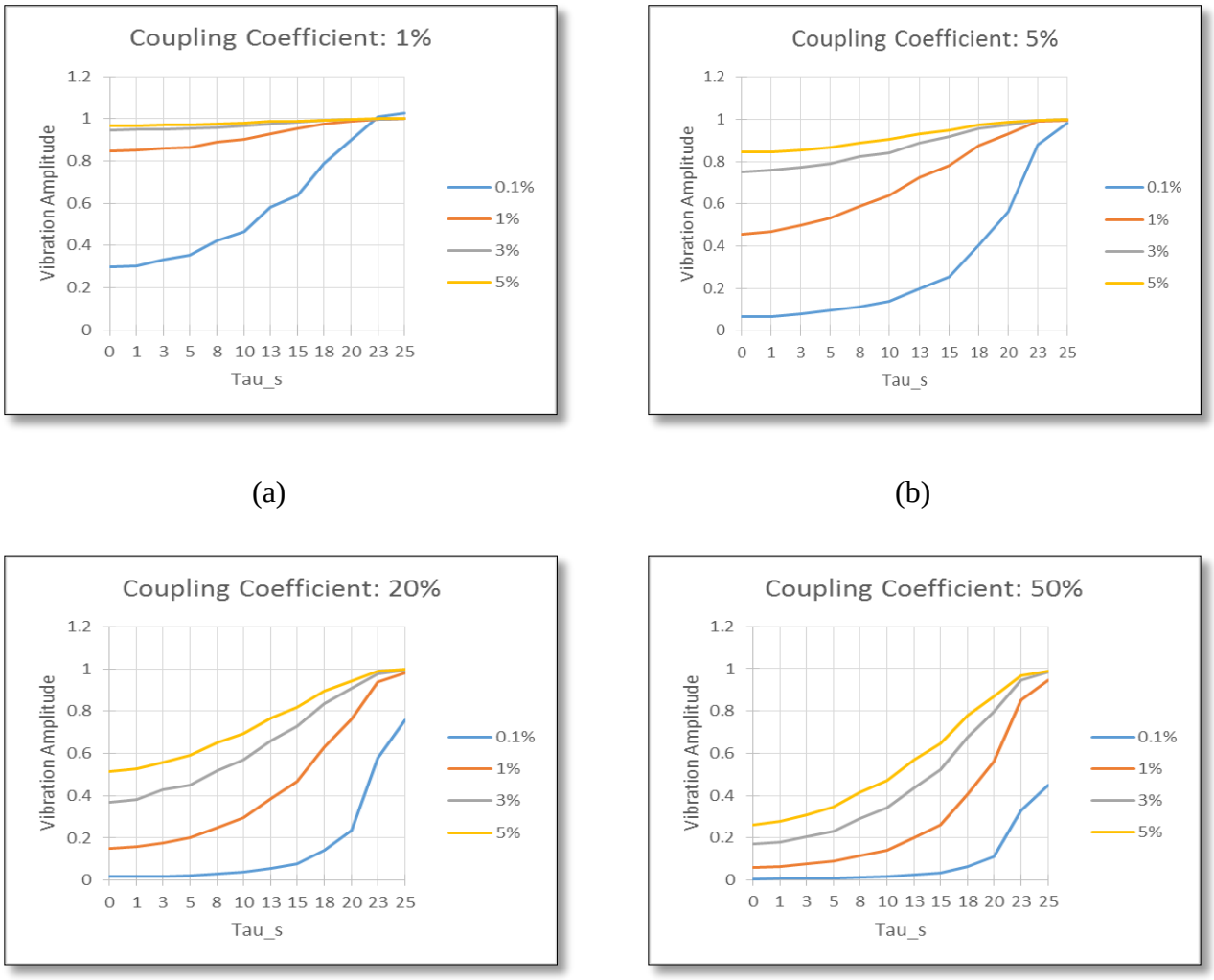

(a) (b)

(c) (d)

Figure 17: Switch Duration Results from Coupled Equation Solver

The plots above show a far greater sensitivity to switch duration than those produced using the results of the initial solver, and display much cleaner trend lines as well. It is noteworthy that

the normalized amplitude on the plots above ends near one for most cases: this indicates that with a 25% switch duration, the State Switching method does not add any damping to the system.

The table below has been produced by examining the data from the coupled equation model. The values of τ represent the characteristic time, as percentage of forcing function period, beyond which 10% increase in vibration amplitude occurs; N/A signifies that vibration amplitudes never increase by more than 10%.

Table 1: Switch Duration Performance Limits

τ_s		Damping			
		0.1%	1%	3%	5%
Coupling	1%	3	15	N/A	N/A
	5%	3	5	10	13
	20%	3	3	5	5
	50%	3	3	3	3

As seen in the table, for low damping the instantaneous switch assumption introduces error in excess of 10% for values of τ_s between 3 and 5%. The two high damping cases, 3 and 5% are far less susceptible to error introduced by the instantaneous assumption; however, for large values of the coupling coefficient, error in excess of 10% is introduced for values of τ_s between 3 and 5% for all damping cases. From the above statements, it is clear that the coupling coefficient plays the dominant role in determining the effects of instantaneous switch assumptions: increasing the value of k^2 drastically increases the error introduced by the instantaneous assumption. The inherent system damping has the opposite effect: in cases where the system overall damping is dominated by inherent damping, the switch duration will have little effect on the overall damping

of the system. Of course, the typical system in which the State Switching method is employed does not have high inherent damping or else the State Switching method would not be required.

5.2 EFFECTS OF SWITCH DELAY

The plots below, like those in Figure 15 and Figure 17 were constructed using the results obtained from the initial solver as well as the coupled equation solver. The format of the plots is identical except switch duration on the horizontal axis is now replaced by switch delay.

In Figure 19 (a) the 0.1% damping line rises above the other damping lines: this is the only case in which the normalized vibration amplitude of the 0.1% damping case surpasses that of the other cases. This anomaly may indicate a drastic decrease in technique performance at high τ_d values for low k^2 values; the higher damping cases are more capable of suppressing the change in damping due to State Switching. This uncharacteristic behavior may also indicate additional insufficiencies in the initial solver; a time domain displacement waveform is shown in Figure 18 for τ_d equals 23%. The waveform below does not indicate issues with the solver; however, the damping lines are not expected to cross in any of the plots.

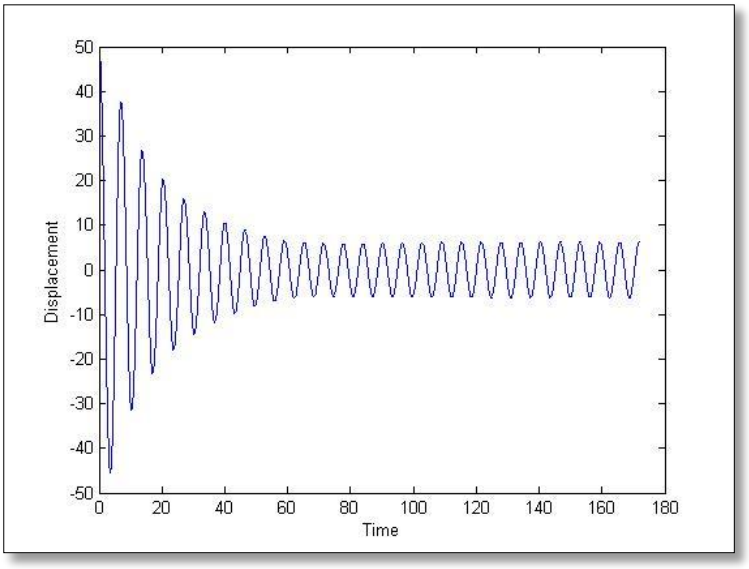

Figure 18: Time Domain Profile for Point Near 0.1% Damping Crossing

There are several points missing on the plots generated by the initial solver: in these cases, the simulation results diverged, so no steady-state (or averaged) vibration amplitude was available. As discussed previously, the initial solver does not prevent the piezoelectric patch from exciting the system for non-ideal conditions. The diverging cases have been removed from the plots as they do not provide insight into the performance of the State Switching technique

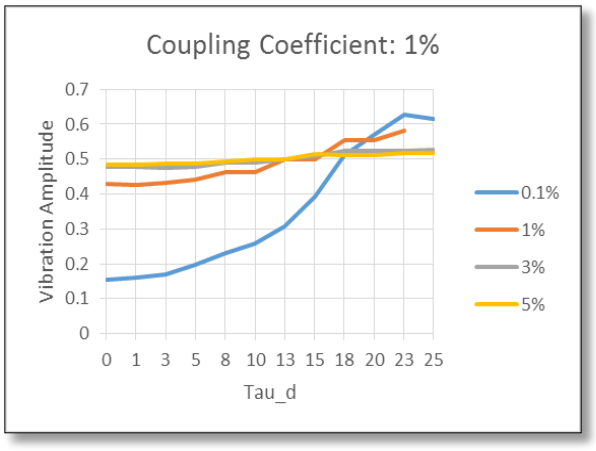

(a)

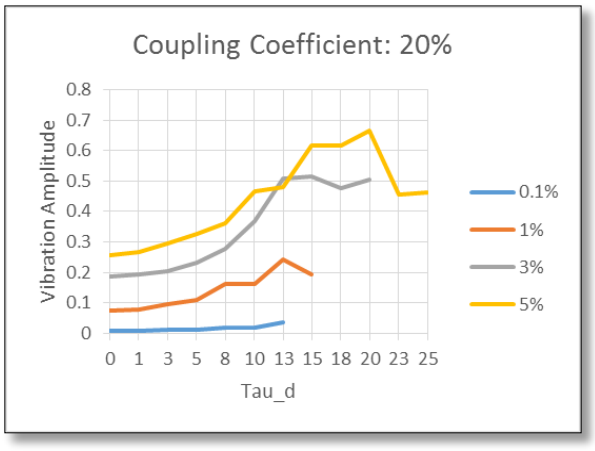

(c)

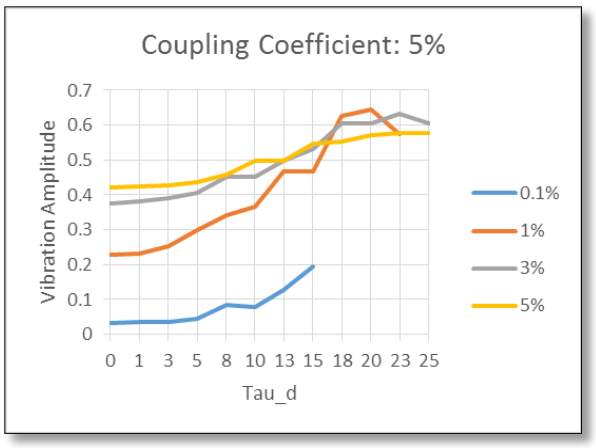

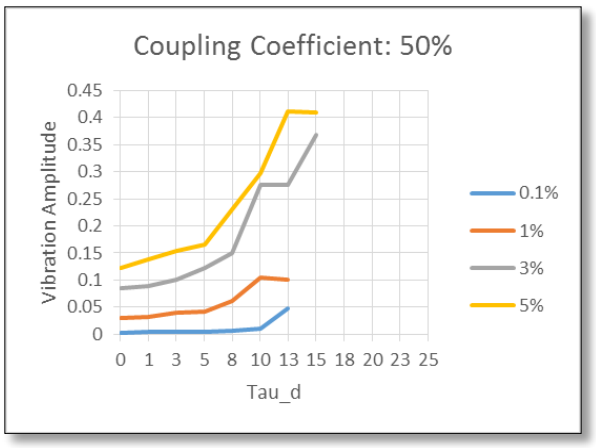

(b) (d)

Figure 19: Switch Duration Results from Initial Solver

The results of the coupled equation solver not only present a much smoother trend line, they illustrate a very different trend. From the plots below, one can conclude that damping will increase for significant switch delays. The trends shown in the figures above are very counter-intuitive, as such a closer look at the time domain is warranted. The first check is the time domain displacement waveform, a typical displacement waveform is shown in Figure 21. All of the plots shown below were created using the same parameter value.

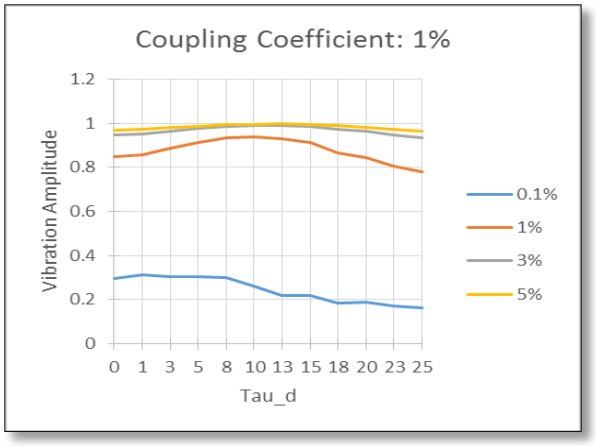

(a)

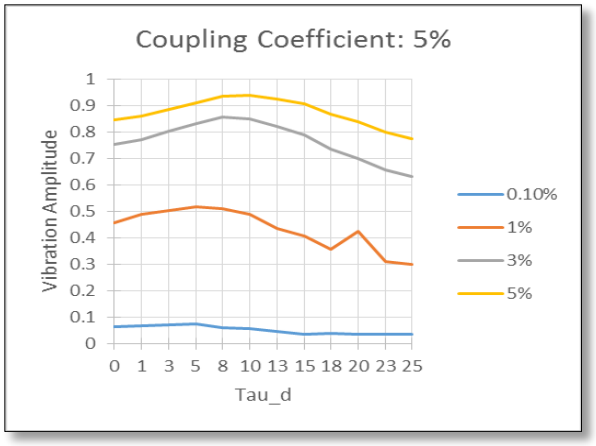

(b)

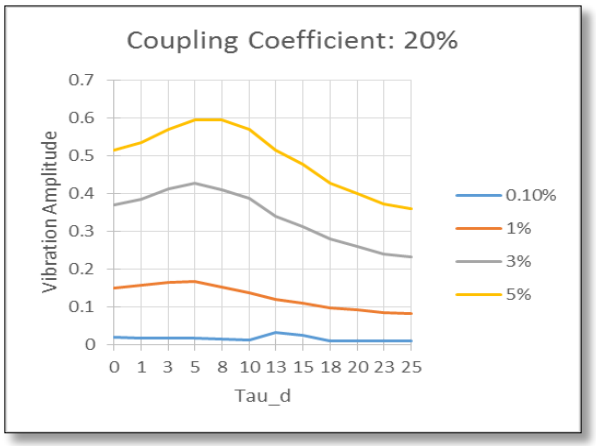

(c)

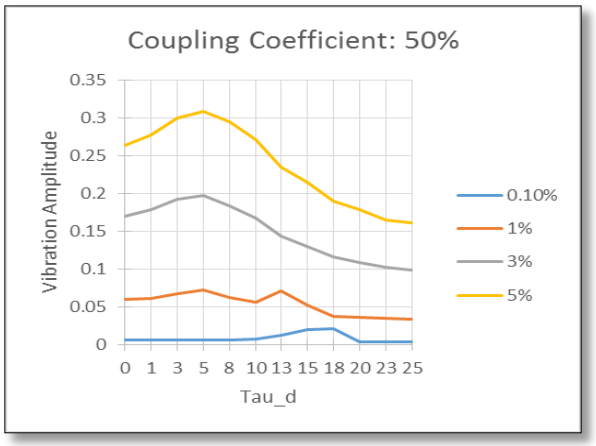

(d)

Figure 20: Switch Delay Results from Coupled Equation Solver

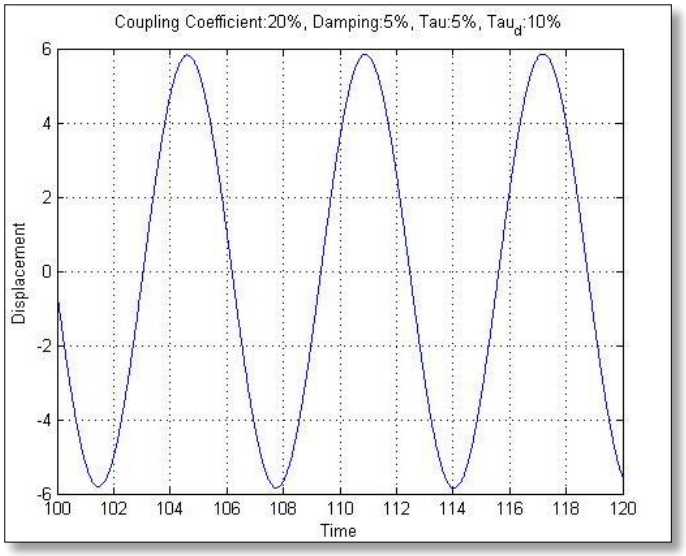

Figure 21: Time Domain Displacement Profile

There is nothing in the time domain displacement waveform which indicates the data is errant. The voltage profile provides a second check; the voltage should be zero when the patch is in the short-circuit state and should mimic the displacement waveform while in the open-circuit state. The transition from short-circuit to open-circuit will not be noticeable; however, the switch from open-circuit to short-circuit should be recognizable by a sharp drop in voltage. A typical time domain voltage waveform is shown aside the corresponding displacement waveform to allow for comparison.

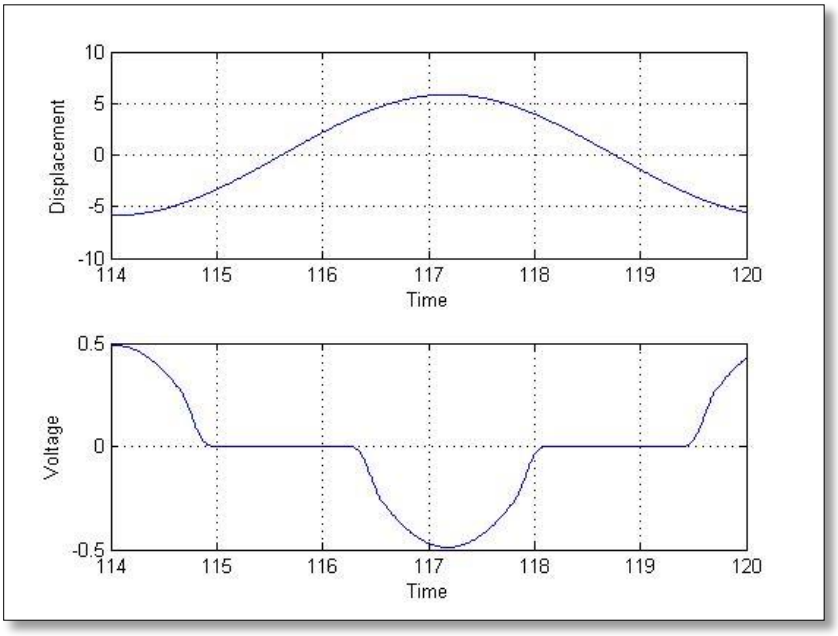

Figure 22: Comparison of Voltage and Displacement

The voltage behaves as expected. The final method of checking the solver results is to examine the charge waveform. The voltage is related to charge through Equation (19): Q is the charge and R the resistance.

$$V = -\dot{Q}R \qquad (19)$$

The voltage profile must be a scaled negative of the charge derivative; a prominent feature of the voltage waveform is the hump that is formed as the voltage mimics the displacement waveform while the patch is in the open-circuit state. The charge profile appears to be flat while the piezoelectric patch is in the open-circuit state, seemingly in conflict with Equation (19). However, closer inspection of the 'flat' segments reveals a third order curve shown in Figure 24. As such, the voltage and charge profiles in Figure 23 agree in light of Equation (19).

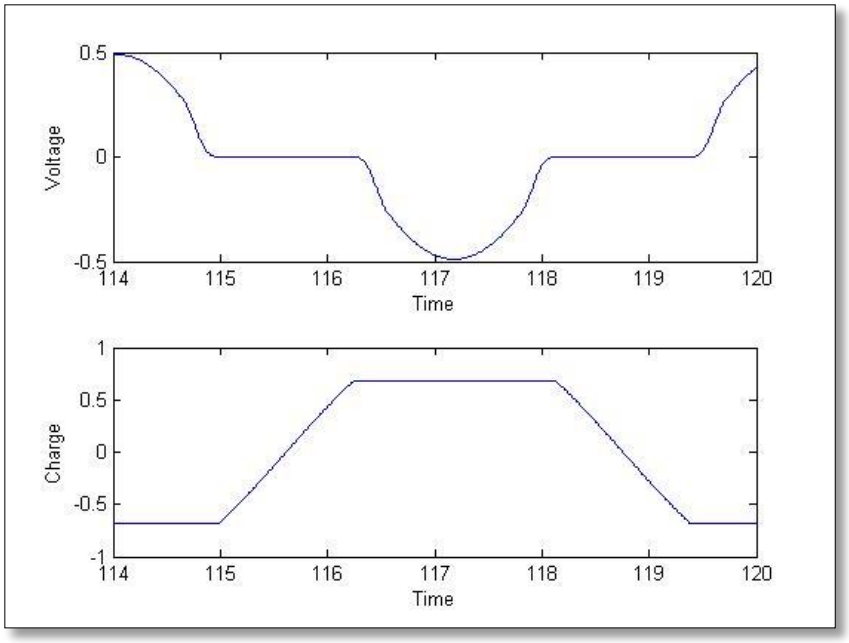

Figure 23: Comparison of Charge and Voltage

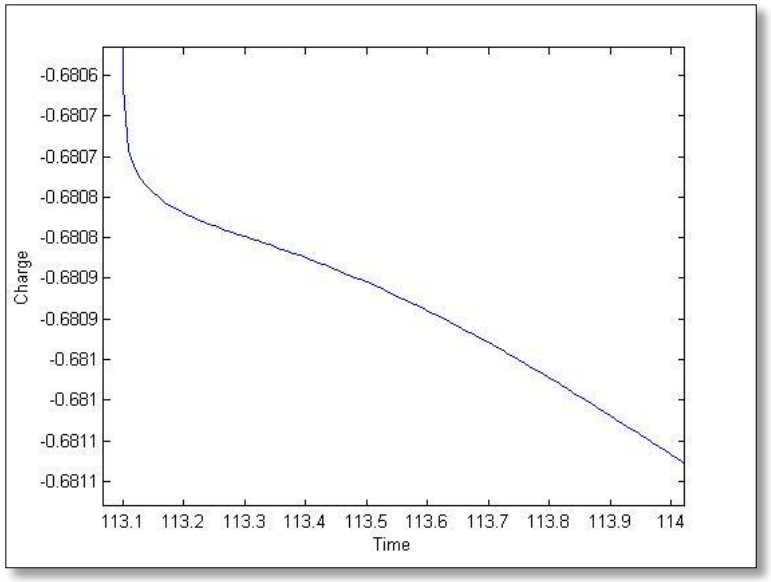

Figure 24: Zoomed Charge Profile

The curvature of the charge during the open-circuit segment is simply difficult to see due to the high non-dimensional resistance (1000) representing the open-circuit state.

The displacement, voltage, and charge profiles show the expected features, indicating that the results of the simulations are correct despite being counter-intuitive. Since the results of the switch delay simulations are still under scrutiny, there will be no table for switch delay such as the one provided in section 5.1.

5.3 COMBINED DURATION AND DELAY

Figure 25 is a surface plot of the steady-state vibration amplitude for particular values of k^2 and ζ as a function of switch duration and switch delay; the values shown in Figure 25 are k^2 equals 5% and ζ equals 3%.

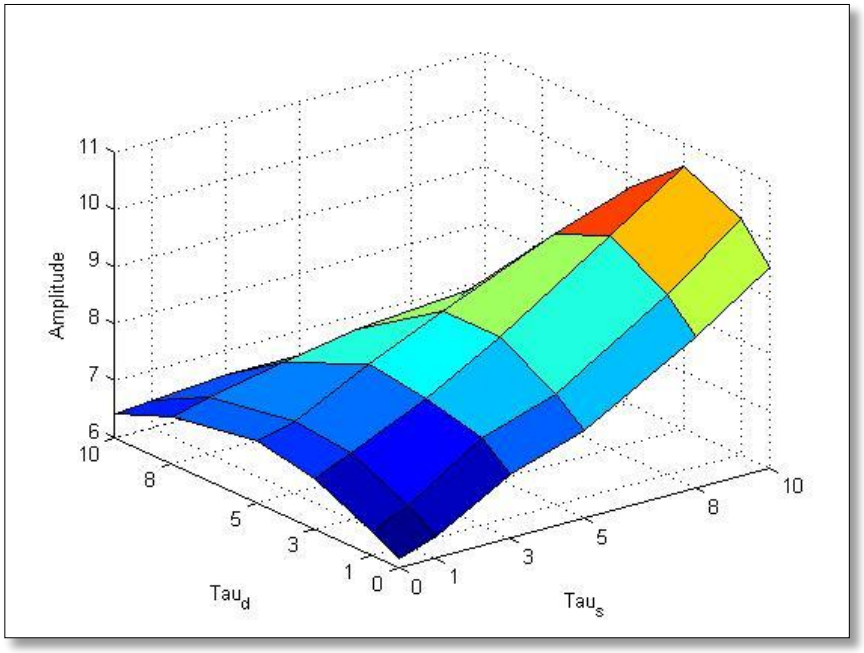

Figure 25: Vibration Amplitude vs. Switch Duration/Delay

Along the x and y planes, the trends shown in the pure duration/delay plots above are visible; however, the vibration amplitude drops for high values of switch duration and switch delay, indicating that the switch delay is the dominating factor in determining steady state vibration amplitude. Similar plots were created for the values of k^2 and ζ used in the pure duration/delay plots; the remaining plots can be found in Appendix A.

5.4 VARIATION WITH RESPECT TO DAMPING AND COUPLING COEFFICIENT

Damping plays several key roles in the simulation that can be clearly seen in the data above. First, all results are normalized using Equation (18); the lower damping values present a much better percent reduction over the non-State Switching damped cases. (However, it is important to note that the results are normalized and do not indicate that State Switching in the presence of lower damping will produce lower absolute vibration amplitudes.) In the plots, this behavior translates into striations: the lines representing different damping values rarely cross.

The electromechanical coupling coefficient has the effect of amplifying plot features: as the coupling coefficient increases, so does the effect of switch duration and delay on vibration reduction. This result is expected: as the coupling coefficient increases, the portion of overall damping contributed by State Switching method increases, so the decrease in damping provided by the State Switching method is more visible.

CHAPTER 6: CONCLUSIONS AND FURTHER RESEARCH

Several conclusions can be drawn from the simulation results provided in Chapter 5 regarding the effects of finite switch time/switch delays on the performance of the State Switching method. These conclusions can be used in designing State Switching dampers and will serve as a starting point for future research. The final chapter is dedicated to drawing conclusions from the data as well as discussing the thought process used to arrive at the conclusion. This thesis by no means presents an exhaustive study on the effects of relaxed assumptions pertaining to the performance of the State Switching damping technique; as such, suggestions for future research will be included at the end of the Chapter. Shortcomings of this research will also be presented to identify key areas where future research could focus to further the understanding of State Switching modeling.

6.1 SIMPLIFIED MODEL VALIDITY

The first conclusion to be drawn from the data is the validity of the simplified model initially used for simulation. As demonstrated in Chapter 5, the initial model was insufficient for both finite switch time and switch delay. The initial solver provided results similar to those produced using the coupled equation solver for pure switch duration; however, there were errant data points. In the case of pure switch delay, the initial solver produced results very dissimilar to those produced using the coupled equation solver. The trends in the data are very different indicating that one of the following is true: the coupled equation solver is incorrect or the initial solver is wholly insufficient.

6.2 LIMIT OF INSTANTANEOUS ASSUMPTIONS

The instantaneous switch assumptions will hold for certain values of the characteristic time parameter. One of the expected results of this research was to determine the range in which the instantaneous assumptions present a reasonable estimate: for this study, vibration amplitude increases of less than 10% are deemed negligible. Determining a range in which the assumptions present an accurate approximation of the true system response will serve in future analysis and system design. Should the allowable characteristic time value exceed the 'typical' characteristic time of the relevant circuitry, the simplified instantaneous system may be used; however, should this not be the case, the characteristic time of the circuitry should be factored into future analysis.

To determine the characteristic time at which performance becomes degraded, the characteristic time value at which vibration amplitude increased by 10% from the instantaneous case was found for each electromechanical coupling coefficient/damping pair. This data was displayed in tabular form in Chapter 5; further discussion and conclusions are presented in the next two sections.

6.2.1 SWITCH DURATION

The plots above show a far greater sensitivity to switch duration than those produced using the results of the initial solver, and display much cleaner trend lines as well. It is noteworthy that the normalized amplitude on the plots above ends near one for most cases: this indicates that with a 25% switch duration, the State Switching method does not add any damping to the system.

The table below has been produced by examining the data from the coupled equation model. The values of τ represent the characteristic time, as percentage of forcing function period, beyond

which 10% increase in vibration amplitude occurs; N/A signifies that vibration amplitudes never increase by more than 10%.

From Table 1, conclusions can be drawn regarding the design of a State Switching device. For low damping and low coupling coefficient, the switch duration should remain less than 3-5% of the forcing function period. The switch duration plays a negligible role in the case of high damping and low coupling coefficient. For the case of high coupling coefficient, τ_{sw} should be kept below 3%, regardless of damping coefficient.

6.2.2 SWITCH DELAY

In order for the instantaneous assumptions to provide an accurate approximation of the system response, switch delays should be in the range of 3-15% of the forcing function period; simulations, and preferably experiments, should be run using application-specific parameter values before designing a State Switching device. Unlike with finite switch time, switch delay cannot be adjusted by circuit tuning alone. For the high frequency excitations experienced in turbines, the voltage of the piezoelectric patch will have to be sampled at a very high rate to ensure the relevant events are detected in a timely manner.

6.2.3 THRESHOLD ENFORCIBILITY

The practicality of design and implementation of devices that meet the criteria for instantaneous assumptions is of great interest. Setting the threshold level for instantaneous analysis to hold true is of no value if technology does not allow the required circuit performance.

Finite switch duration, as shown above, has little effect on the response of the system for values of τ below 15%. Careful selection of the device passive components will ensure that the circuit characteristic time is kept below the threshold; the resistance and capacitance values required should be attainable without exceeding the size requirements for a potential on-blade piezoelectric device. The performance threshold for switch delays may prove more challenging to the designer. The performance of the State Switching technique may decrease drastically for values of τ greater than 3%. Taking 5 kHz as a typical excitation frequency for turbomachinery, the sampling rate would have to be in excess of 160 kHz to ensure the events are captured before the maximum allowable time has passed for optimum system damping. With the size and weight restrictions of an on-blade piezoelectric device, achieving such high sampling rates may present quite a challenge. If the requirements cannot be met, the switch delay must be factored into all analyses.

6.3 FUTURE WORK

No research is complete in the examination of a topic; as such, this section lays out a potential path for future research. There are several directions that should be considered, including further analysis via simulation, validation via physical experiments, and applied testing via practical implementation. Each of these areas would provide useful information for the development of piezoelectric damping devices.

6.3.1 FUTURE SIMULATION

As discussed in Chapter 4, the case of τ greater than 25% was not handled in this body of work. It would be interesting, and possibly beneficial, to ascertain the behavior of a piezoelectric patch when the switch is reversed before being completed, in the case of finite switch duration, or when the switch is initiated out of phase with the patch displacement, as in the case of a switch delay. Knowledge of the patch behavior, and response simulation, for large deviations from design conditions may allow for the development of techniques that maintain damping performance in atypical operating conditions.

A second area of investigation lies in the modified delay model. The coupled equation solver may be modified to handle pure switch delays, in which case the system response can be compared to the data from the modified delay solver, presented in Chapter 5. The coupled equation solver was used for the finite time duration simulations because directly varying the stiffness state did not accurately represent the process in a physical system; however, directly varied stiffness in the case of a pure switch delay should be sufficient to produce accurate response approximations.

The models presented in Chapter 3 and the Appendix may only be used for the State Switching method; however, they could be modified to handle other piezoelectric-based damping techniques such as those of the Synchronized Switch Damping family. There is still opportunity to explore these techniques further, and it could be especially useful for the Synchronized Switch Damping on an Inductor since any delays or switch duration can dramatically impact the sizing of the inversion circuit components. Creating a properly tuned circuit may require large inductors and resistors.

6.3.2 EXPERIMENTAL VALIDATION

Simulations alone should not provide the sole source of information when drawing conclusions about physical processes: there are far too many processes present in a physical event for a model to reproduce the system response exactly. As such, it is important that all models be verified through experimentation with the physical system. To verify the assumptions made earlier in the Chapter, a series of tests should be conducted on a State Switching device such that the simulation results are definitively confirmed or rejected.

The finite switch duration results should be verified by replacing the shunt with a variable resistor, through which the resistance of the circuit can be controlled to institute a gradual transition between the open and short-circuit cases. The experiments should be conducted at low frequencies to increase switch time for a given value of τ_{sw}, which should allow for more control over the transition.

The switch delay case can be tested by simply modifying the control methods of the State Switching device. Again, the test should be conducted at low frequencies to allow for greater control over the switch delay.

6.3.3 PRACTICAL APPLICATION

For the purpose of this thesis, 10% error was set as the limit of 'negligible'; however, there may be applications in which error in excess of 10% is also negligible. There may be other applications in which errors less than 10% are excessive. With experimental validation and improvement upon the presented models, designers will have the opportunity to select the key

parameter values and determine the error limits for specific applications. This knowledge will expand the reach of this research and improve the design process for State Switching devices.

APPENDIX A

Surface plots for Combination Switch Duration/Delay

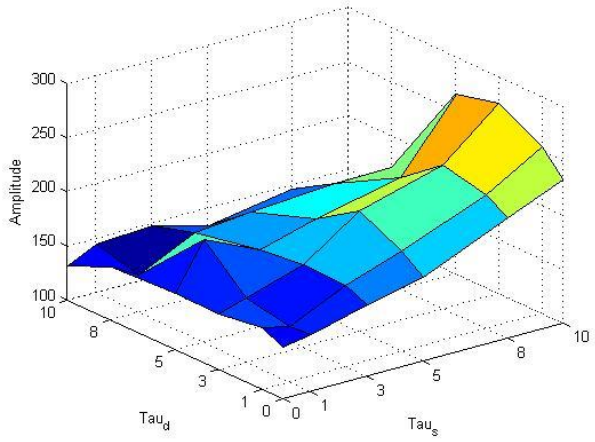

(a)

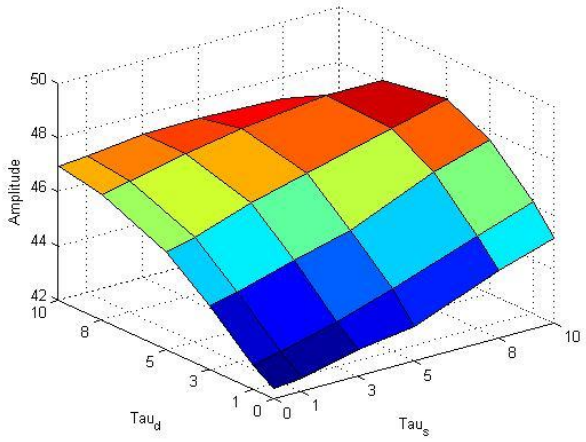

(b)

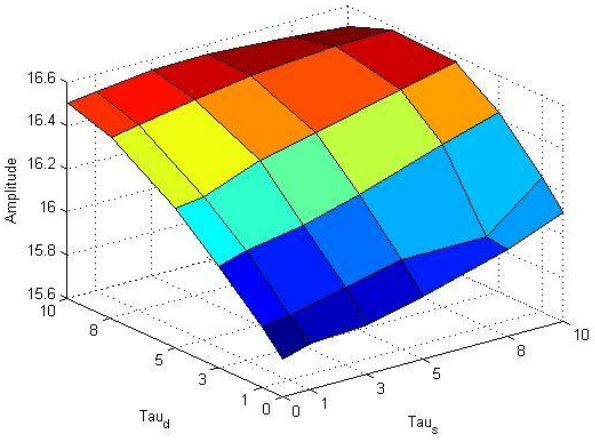

(c)

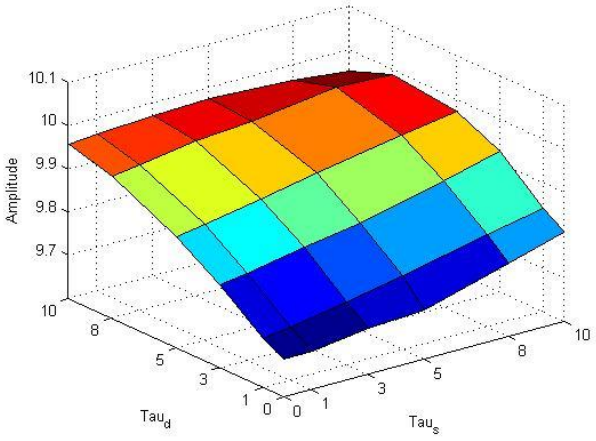

(d)

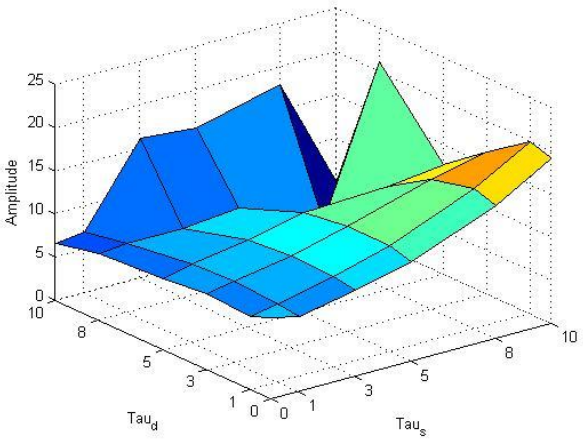
Amplitude
25
20
15
10
5
0
10
8
5
3
1
0
Tau_d
0
1
3
5
8
10
Tau_s

(e)

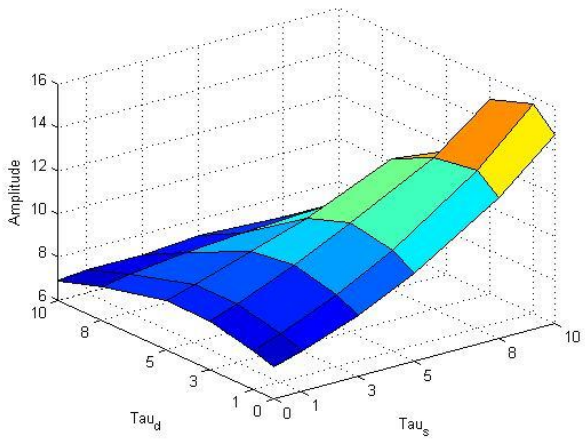
Amplitude
16
14
12
10
8
6
10
8
5
3
1
0
Tau_d
0
1
3
5
8
10
Tau_s

(f)

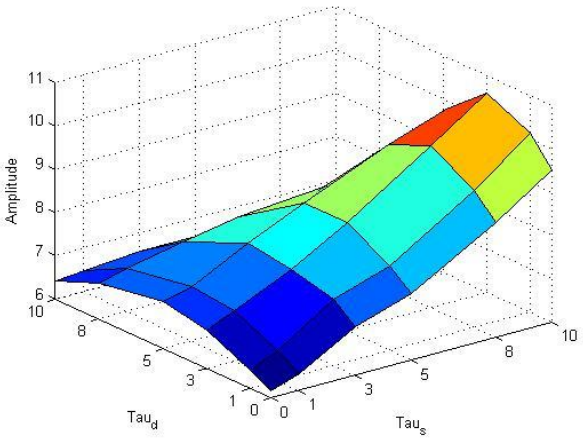
Amplitude
11
10
9
8
7
6
10
8
5
3
1
0
Tau_d
0
1
3
5
8
10
Tau_s

(g)

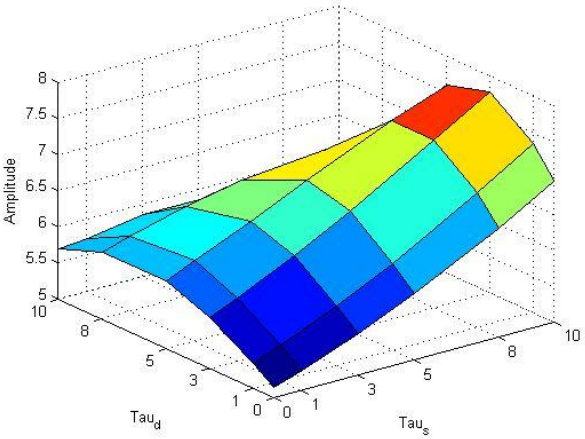
Amplitude
8
7.5
7
6.5
6
5.5
5
10
8
5
3
1
0
Tau_d
0
1
3
5
8
10
Tau_s

(h)

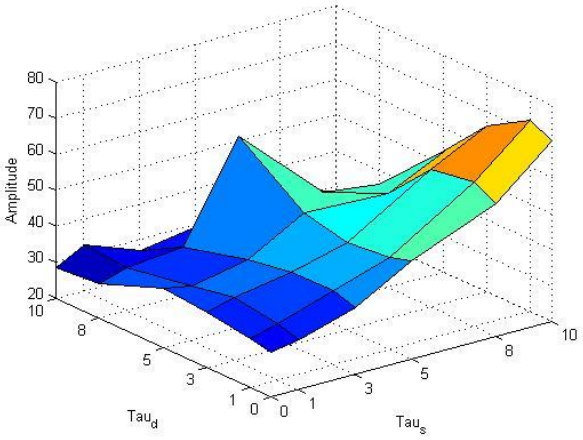
Amplitude
80
70
60
50
40
30
20
10
8
5
3
1
0
Tau_d
0
1
3
5
8
10
Tau_s

(i)

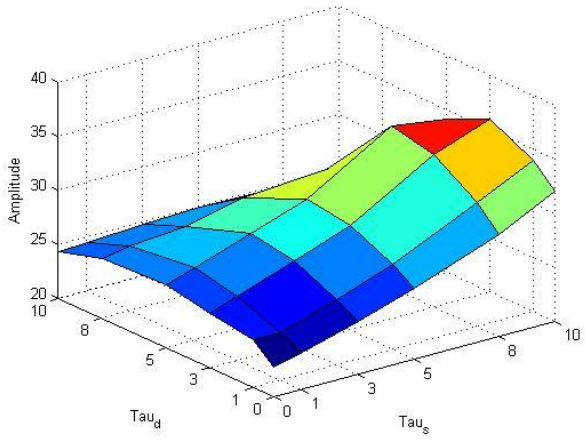
Amplitude
40
35
30
25
20
10
8
5
3
1
0
Tau_d
0
1
3
5
8
10
Tau_s

(j)

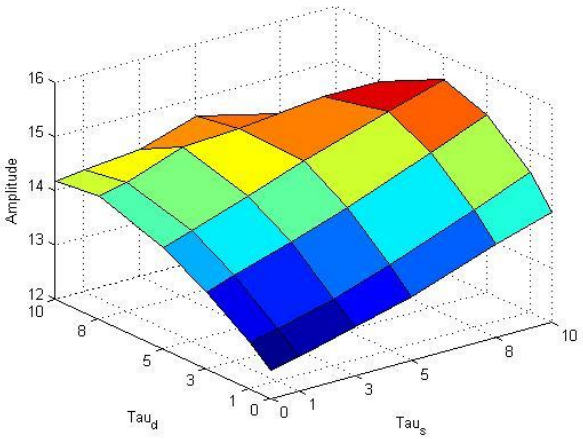
Amplitude
16
15
14
13
12
10
8
5
3
1
0
Tau_d
0
1
3
5
8
10
Tau_s

(k)

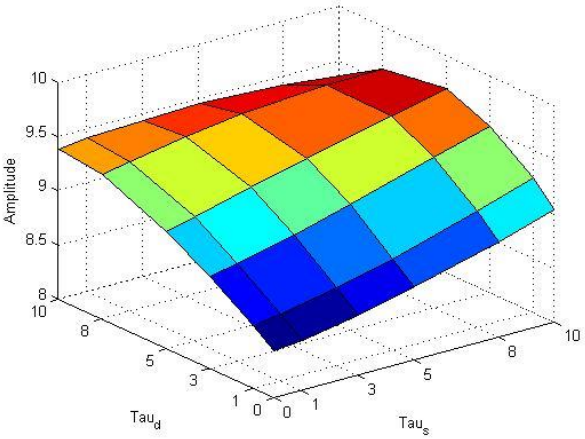
Amplitude
10
9.5
9
8.5
8
10
8
5
3
1
0
Tau_d
0
1
3
5
8
10
Tau_s

(l)

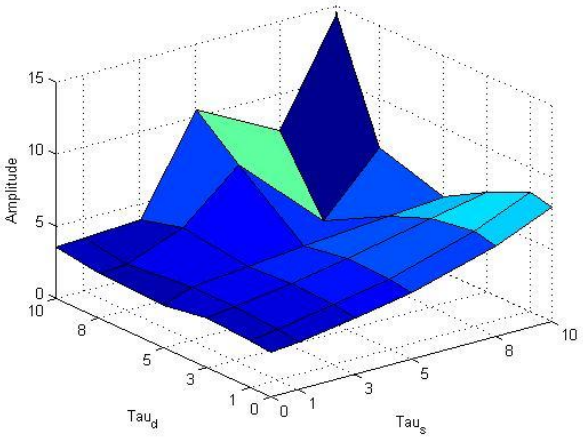

(m)

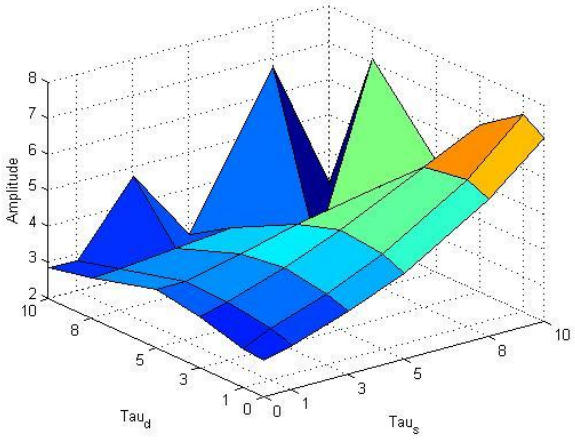

(n)

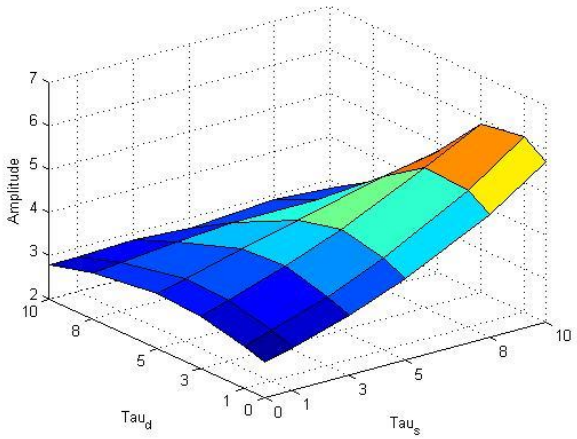

(o)

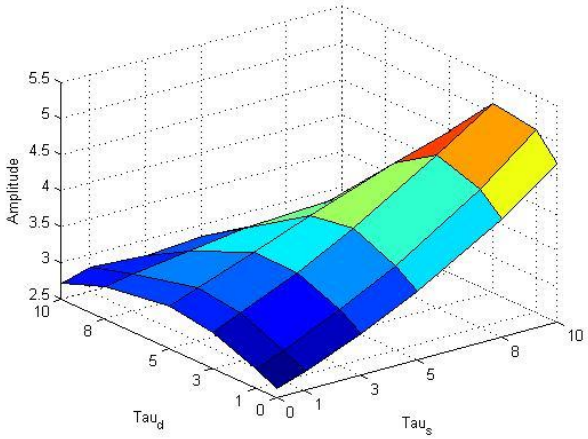

(p)

		Damping			
		0.1%	1%	3%	5%
Coupling	1%	a	b	c	d
	5%	e	f	g	h
	20%	i	j	k	l
	50%	m	n	o	p

APPENDIX B

Matlab Code

Initial Solver

```
function out = solver(tau_p,tau_dp,k_squared,zeta)

%time each run
e = cputime;

%System parameters not included in the test matrix
omega = 1;
f_period = 2*pi/omega;

%Parameters derived from test matrix parameters
tau = f_period*tau_p/100;
tau_d = f_period*tau_dp/100;

%Set initial time window and step size for ODE45
final = 50*f_period;
step = 0.01;
t_start = 0;
tspan = (t_start:step:final);

%Set initial conditions
%est = 1/(2*zeta);
initial = [50;0];
inits = transpose(initial);

%Set convergence criteria
stop = 1E-3;

%Set up ODE45 Events and initialize events output matrices
options = odeset('Events',@events);
yout = inits;
test = false;
tout = 0;
teout = [];
yeout = [];
ieout = [];
y_max = [];
ie = 1;

%Loop runs simulation until convergence criteria are met or until timeout
while test==false
[t,y,te,ye,ie] =
ode45(@EOM,tspan,initial,options,zeta,omega,tau,t_start,k_squared,ie,tau_d);

%store output data
nt = length(t);
tout = [tout; t(2:nt)];          %time output of ode solver
yout = [yout; y(2:nt,:)];        %[displacement,velocity] output of ode solver
```

```
teout = [teout; te];            %time of events
yeout = [yeout; ye];            %[displacement,velocity] for events
ieout = [ieout; ie];            %event # found

%test if convergence criteria are met
if ie==1                    %velocity = 0 and decreasing
y_max = [y_max;yout(end,1)];    %vector containing peak values
    if  length(y_max)>2 && abs(y_max(end)-y_max(end-1))<=stop   %if more than
two peaks have been recorded and convergence criteria is met, stop
        test = true;
    end
end

%End if timeout or solution diverges
result = 'converge';
if yout(end)>1000           %if solution diverges, stop
    test = true;
    result = 'diverge';
elseif t_start>1000         %if simulation reaches 1000 seconds, stop
    test = true;
    result = 'timeout';
end

%Set new time window for ODE45
initial = (yout(end,:));
t_start = tout(end);
final = t_start + 50*f_period;
tspan = (t_start:step:final);

end

plot(tout,yout(:,1),'b')

%save results
if length(tout)>100000
    out.time = tout(end-100000:end,1);
    out.Displacement = yout(end-100000:end,1);
    out.Velocity = yout(end-100000:end,2);
else
    out.time = tout(:,1);
    out.Displacement = yout(:,1);
    out.Velocity = yout(:,2);
end
out.Peaks = yeout(:,1);
out.Tau = tau_p;
out.Tau_d = tau_dp;
out.ksquared = k_squared;
out.Damping = zeta;
out.Result = result;

%Compare start and end time to find time taken to run solver
computation_time = cputime - e
```

```
%end Solver
end

%EOM function: defines motion for ode solver; variable stiffness states
%defined
function y = EOM( t,x,zeta,omega,tau,t_start,k_squared,ie,tau_d,f_period)
diff = t-t_start;
    if ie==2                                        %zero crossing
        if diff<tau_d                               %before switch
            S = 1-k_squared;
        elseif diff>tau_d && diff<tau_d+tau         %during switch
            A = -2*k_squared/(tau^3);
            B = -3/2*A*tau;
            C = 0;
            D = 1-k_squared;
            S = A*diff^3+B*diff^2+C*diff+D;
        else                                         %after switch
            S = 1;
        end
    else                                             %max or min
        if diff<tau_d                                %before switch
            S = 1;
        elseif diff>tau_d && diff<tau_d+tau          %during switch
            A = 2*k_squared/(tau^3);
            B = -3/2*A*tau;
            C = 0;
            D = 1;
            S = A*diff^3+B*diff^2+C*diff+D;
        else                                         %after switch
            S = 1-k_squared;
        end
    end
y = [];
y = [x(2);-S*x(1)+cos(omega*t)-2*zeta*x(2)];
end


%events function: defines events to be recognized by ode solver
function [value,isterminal,direction] =
events(t,y,zeta,omega,tau,t_start,k_squared,ie,tau_d,f_period)
    value = [y(2),y(1),y(2)];              %event when velocity or
displacement hits zero
    isterminal = [1,1,1];                   %stops integration
    direction = [-1,0,1];                  %velocity decreasing at y_max,y =
0,velocity increasing at y_min
end
```

Coupled Equation Solver

```
function out = coupled(tau_p,tau_dp,k_squared,zeta)
```

```
% Solver uses the coupled differential equations, solving for the term Q:
% Resistance, Q, and Q_dot are then used to produce the displacement
% vector. Pertinent values are saved to a structure.

e = cputime;

%System parameters not included in the test matrix
omega = 1;
f_period = 2*pi/omega;

%Parameters derived from test matrix parameters
tau = f_period*tau_p/100;
tau_d = tau_dp*f_period/100;

%Set initial time window and step size for ODE45
final = 50*f_period;
step = 0.01;
t_start = 0;
tspan = (t_start:step:final);

%Set initial conditions
initial = [1;0;0];

%Set convergence criteria
stop = 1E-3;

%Set up ODE45 Events and initialize events output matrices
options = odeset('Events',@even);
yout = transpose(initial);
test = false;
tout = 0;
teout = [];
yeout = [];
ieout = [];
y_max = [];
ie = 1;

%Loop runs simulation until convergence criteria are met or until timeout
while test==false
[t,y,te,ye,ie] =
ode45(@EOM,tspan,initial,options,zeta,tau,tau_d,t_start,k_squared,ie);

%store output data
nt = length(t);
tout = [tout; t(2:nt)];          %time output of ode solver
yout = [yout; y(2:nt,:)];        %[Q,Q_dot,Q_doubledot,Q_tripledot] output of
ode solver
teout = [teout; te];             %time of events
yeout = [yeout; ye];             %[displacement,velocity] for events
ieout = [ieout; ie];             %event # found

%test if convergence criteria are met
```

```
if ie==1                    %velocity = 0 and decreasing
y_max = [y_max;yout(end,1)];    %vector containing peak values
    if  length(y_max)>2 && abs(y_max(end)-y_max(end-1))<=stop   %if more than
two peaks have been recorded and convergence criteria is met, stop
        test = true;
    end
end

%End if timeout or solution diverges
result = 'converge';
if max(abs(yout))>1000          %if solution diverges, stop
    test = true;
    result = 'diverge';
elseif t_start>5000         %if simulation reaches 1000 seconds, stop
    test = true;
    result = 'timeout';
end

%Set new time window for ODE45
initial = (yout(end,:));
t_start = tout(end);
final = t_start + 50*f_period;
tspan = (t_start:step:final);

end

%plot results
h(1)=subplot(212);
plot(tout,yout(:,1),'b')
h(2)=subplot(211);
plot(teout,ieout,'ro-');

%re-create R
ie = 1;
Res = [];
t_start = 0;
for i = 1:length(tout)
    t = tout(i);
    for j = 1:length(teout)
        if t==teout(j)
            ie = ieout(j);
            t_start = t;
        end
    end
    diff = t-t_start;
    if ie==2                                    %low to high
        if diff<tau_d
            R = 0.001;
        elseif diff>tau_d && diff<tau_d+tau
            A = -2*(1000-0.001)/tau^3;
            B = -3/2*A*tau;
            C = 0;
            D = 0.001;
```

```
            R = A*(diff-tau_d)^3+B*(diff-tau_d)^2+C*(diff-tau_d)+D;
        else
            R = 1000;
        end
    else                                            %high to low
        if diff<tau_d
            R = 1000;
        elseif diff>tau_d && diff<tau_d+tau
            A = -2*(0.001-1000)/tau^3;
            B = -3/2*A*tau;
            C = 0;
            D = 1000;
            R = A*(diff-tau_d)^3+B*(diff-tau_d)^2+C*(diff-tau_d)+D;
        else
            R = 0.001;
        end
    end
Res = [Res;R];
end

%find Voltage
V = [];
for i = 1:length(Res)
    V = [V;-((-yout(i,3)+k_squared*yout(i,1))/R)*Res(i)];
end

%save results
if length(tout)>100000
    out.time = tout(end-100000:end,1);
    out.Displacement = yout(end-100000:end,1);
    out.Velocity = yout(end-100000:end,2);
    out.Charge = yout(end-100000:end,3);
    out.Resistance = Res(end-100000:end,1);
    out.Voltage = V(end-100000:end,1);
else
    out.time = tout(:,1);
    out.Displacement = yout(:,1);
    out.Velocity = yout(:,2);
    out.Charge = yout(:,3);
    out.Resistance = Res(:,1);
    out.Voltage = V(:,1);
end
out.Tau = tau_p;
out.Tau_d = tau_dp;
out.ksquared = k_squared;
out.Damping = zeta;
out.Result = result;
out.te = teout(:,1);
out.ie = ieout(:,1);
out.ye = yeout(:,1);


%Compare start and end time to find time taken to run solver
```

```
computation_time = cputime - e

%end Solver
end

%EOM function: defines motion for ode solver; variable stiffness states
%defined
function y = EOM( t,x,zeta,tau,tau_d,t_start,k_squared,ie)
diff = t-t_start;
%Resistance switching function
if ie==2                                        %low to high
    if diff<tau_d
        R = 0.001;
    elseif diff>tau_d && diff<tau_d+tau
        A = -2*(1000-0.001)/tau^3;
        B = -3/2*A*tau;
        C = 0;
        D = 0.001;
        R = A*(diff-tau_d)^3+B*(diff-tau_d)^2+C*(diff-tau_d)+D;
    else
        R = 1000;
    end
else                                            %high to low
    if diff<tau_d
        R = 1000;
    elseif diff>tau_d && diff<tau_d+tau
        A = -2*(0.001-1000)/tau^3;
        B = -3/2*A*tau;
        C = 0;
        D = 1000;
        R = A*(diff-tau_d)^3+B*(diff-tau_d)^2+C*(diff-tau_d)+D;
    else
        R = 0.001;
    end
end
y = [x(2);sin(t)+x(3)-x(1)-2*zeta*x(2);(-x(3)+k_squared*x(1))/R];
end


%events function: defines events to be recognized by ode solver
function [value,isterminal,direction] =
even(t,y,zeta,tau,tau_d,t_start,k_squared,ie)
    value = [y(2),y(1),y(2)];             %event when velocity or
displacement hits zero
    isterminal = [1,1,1];                  %stops integration
    direction = [-1,0,1];                 %velocity decreasing at y_max,y =
0,velocity increasing at y_min
end
```

LIST OF REFERENCES

[1] Webster Inc., The Marriam-Webster Dictionary, Springfield: Merriam-Webster, 2004.

[2] R. Hibbeler, Mechanics of Materials, Boston: Prentice Hall, 2011.

[3] W. H. Warnes, "ENGR322: Final Exam Winter 1999," Oregon State, 18 March 1999. [Online]. Available: http://oregonstate.edu/instruct/engr322/Exams/Previous/W99/ENGR322Final.html. [Accessed 28 June 2014].

[4] S. S. Rao, Mechanical Vibrations, Upper Saddle River: Pearson Education, 2011.

[5] D. Morrow and S. Lust, "Using Tuned Mass Dampers in an Optical Assembly," in *Curran Associates, Inc.*, Kissimmee, 2003.

[6] A. Afsharfard and A. Farshidianfar, "Modeling and analysis of magnetorheological inner mass single unit impact dampers," *Journal of Intelligent Material Systems and Structures*, vol. 25, no. 3, pp. 342-351, 2013.

[7] T. Korakianitis, "On the Propogation of Viscous Wakes and Potential Flow in Axial-Turbine Cascades," *Journal of Turbomachinery*, vol. 115, no. 1, pp. 118-127, 1993.

[8] K. Anup, T. Bhola and L. Young-Ho, "Transient numerical analysis of rotor–stator interaction in a Francis turbine," *Renewable Energy*, vol. 65, pp. 227-235, 2014.

[9] C. M. Firrone and S. Zucca, "Modelling Friction Contacts in Structural Dynaimcs and its Application to Turbine Bladed Disks," in *Numerical Analysis - Theory and Application*, Rijeka, InTech, 2011.

[10] K. Sanliturk, D. Ewins, R. Elliott and J. Green, "Friction Damper Optimization: Simulation of Rainbow Tests," *Journal of Engineering for Gas Turbines and Power,* vol. 123, no. 4, pp. 930-939, 1999.

[11] T. Giampaolo, Gas Turbine Handbook Principles and Practices, Lilburn: Fairmont Press Inc., 2006.

[12] Mitsubishi Hitachi Power Systems, "Products," Mitsubishi Hitachi Power Systems, [Online]. Available: http://mpshq.com/gas-turbines.html. [Accessed 28 May 2014].

[13] D. Secenekleri, "Research Interests," Middle Eastern Technological University, 17 February 2014. [Online]. Available: http://www.metu.edu.tr/~ender/Research.htm. [Accessed 30 May 2014].

[14] J. Szwedowicz, "30 Year Anniversary of Friction Damper Technology in TUrbine Blades," *Mechanical Engineering,* vol. 132, no. 4, pp. 54-55, 2010.

[15] J. Roberts and P. Popper, Piezoelectric Ceramics, New York: Academic Press Inc., 1971.

[16] J. Valdovinos, R. Williams, D. S. Levi and G. P. Carman, "Evaluating piezoelectric hydraulic pumps as drivers for pulsatile pediatric ventricular assist devices," *Journal of Intelligent Material Systems and Structures,* vol. 25, no. 10, pp. 1276-1285, 2013.

[17] "PCBMotor," [Online]. Available: http://pcbmotor.com/images/basicstator.gif. [Accessed 25 March 2014].

[18] N. W. Hagood and A. von Flotow, "Damping of structural vibrations with piezoelectric materials and passive electrical networks," *Journal of Sound and Vibration,* vol. 146, no. 2, pp. 243-268, 1991.

[19] K. Lau, D. E. Quevedo, B. J. Vautier, G. C. Goodwin and S. Moheimani, "Design of modulated and demodulated controllers for flexible structures," *Control Engineering Practice,* vol. 15, no. 3, pp. 377-388, 2007.

[20] W. Clark, "Vibration Control with State-Switched Piezoelectric Materials," *Journal of Intelligent Material Systems and Structures,* vol. 11, pp. 263-271, 2000.

[21] C. Richard, D. Guyomar, D. Audigier and G. Ching, "Semi-passive damping using continuous switching of a piezoelectric device," in *SPIE Conference on Passive Damping and Isolation*, Newport Beach, 1999.

[22] C. Richard, D. Guyomar, D. Audigier and H. Bassaler, "Enhanced semi-passive damping using Continuous switching of a piezoelectric device on an inductor," in *Smart Structures and Materials 2000: Damping and Isolation*, Newport Beach, 2000.

[23] E. Lefeuvre, A. Badel, L. Petit, C. Richard and D. Guyomar, "Semi-passive piezoelectric structural damping by synchronized switching on adaptive voltage sources," *Journal of Intelligent Material Systems and Structures,* vol. 17, no. 8-9, pp. 653-660, 2006.

[24] L. R. Corr and W. W. Clark, "Comparison of low-frequency piezoceramic shunt techniques for structural damping," in *Smart Structures and Materials 2001: Damping and Isolation*, Newport Beach, 2001.

[25] J. Kauffman and G. Lesieutre, "Piezoelectric-based Vibration Reduction of Turbomachinery Bladed Disks via Resonance Frequency Detuning," *AIAA Journal,* vol. 50, no. 5, pp. 1137-1144, 2012.

[26] H. P. Bloch, "Selecting steam turbines in a 'lean' environment," 1 February 2012. [Online]. Available: http://www.hydrocarbonprocessing.com/Article/2972983/Selecting-steam-turbines-in-a-lean-environment.html. [Accessed 3 July 2014].

[27] Piezo Systems Inc., "Piezo Terminology," 2011. [Online]. Available: http://www.piezo.com/tech1terms.html. [Accessed 3 July 2014].

[28] K. Sanliturk, D. Ewins and A. Stanbridge, "Underplatform Dampers for Turbine Blades: Theoretical Modeling, Analysis, and Comparison with Experimental Data," *Journal of Engineering for Gas Turbines and Power,* vol. 123, no. 4, pp. 919-929, 1998.